

Semi-inclusive two-nucleon emission in (anti) neutrino charged current scattering within the relativistic mean field framework

V. L. Martinez-Consentino , A. M. Cantizani, and J. E. Amaro 

Departamento de Física Atómica, Molecular y Nuclear, and Instituto de Física Teórica y Computacional Carlos I, Universidad de Granada, Granada 18071, Spain



(Received 19 October 2023; accepted 11 December 2023; published 8 January 2024)

This paper delves into the distribution of semi-inclusive events involving the emission of two nucleons in (anti) neutrino charged-current scattering. The analysis is conducted within the framework of relativistic mean-field theory applied to nuclear matter. To quantify the likelihood of such semi-inclusive events occurring, we employ a relativistic model of meson-exchange currents that aligns with the 2p2h inclusive cross section. The outcomes are presented in terms of onefold and twofold integrated semi-inclusive cross sections. To highlight disparities among the various emission channels, including proton-proton, neutron-proton, and neutron-neutron, we compare them against a purely phase-space isotropic distribution within the center of mass of the two nucleons. These comparisons reveal significant differences in the event distributions, shedding light on the distinctive characteristics of each channel.

DOI: [10.1103/PhysRevC.109.015502](https://doi.org/10.1103/PhysRevC.109.015502)

I. INTRODUCTION

The investigation of multinucleon emission reactions induced by neutrinos and other electroweak probes has garnered significant attention in contemporary physics [1–6]. This heightened interest stems from the compelling evidence of its presence within the quasielastic (QE) peak region, where a substantial contribution of two-nucleon emission coexists with one-nucleon knockout events, defying disentanglement in inclusive experiments. In other words, in this context, the precise final hadronic state is largely unknown, except for the possible absence of pions. This intriguing phenomenon has been underscored in the analysis of neutrino and antineutrino scattering experiments [7–10].

The significance of 2p2h processes in the inclusive cross section has been underscored and substantiated through theoretical investigations by various research groups [11–14]. These studies employ diverse models that incorporate various nuclear effects, such as meson-exchange currents (MECs) with Δ -isobar excitations, final-state interactions (FSIs), short-range correlations (SRCs), the random-phase approximation (RPA), and effective interactions. These models encompass a range of approaches, including Fermi gas models, which can be either local or global and may incorporate relativistic corrections. Other approaches, on the other hand, utilize shell models or quantum hadrodynamics models [15–17]. *Ab initio* methods also have unveiled that

MEC exert a substantial influence on the transverse response, a phenomenon consistent with the significant presence of 2p2h excitations. However, it is worth noting that, in these calculations, the contribution from distinct final states cannot be readily disentangled [18,19]. In the factorization scheme, which relies on the spectral function formalism, a similar contribution attributed to 2p2h excitations has also been identified [20]. However, the inclusion of these model-dependent ingredients has resulted in noticeable disparities among the theoretical predictions. As a consequence, numerous research endeavors have aimed to compare the results to elucidate and mitigate the systematic uncertainties inherent in neutrino data analyses [21–24].

This situation has necessitated the integration of two-nucleon ejection mechanisms into Monte Carlo (MC) neutrino event generators [25]. Typically, one commences with only the inclusive cross-section information in the 2p2h channel, as provided by theoretical groups, and lacks the corresponding semi-inclusive cross-section data. In the absence of specific knowledge regarding the distribution of the two final particles, it has become imperative to resort to reasonable prescriptions for implementing an algorithm that generates events with two-nucleon final states, based on given values of momentum and energy transfer. The conventional approach [26–29] involves selecting two nucleons from the Fermi sea. By ensuring energy-momentum conservation, the four-momentum of the final hadronic state (comprising two nucleons) can be computed. A reasonable assumption, in the absence of more specific information, is to consider that the distribution of the two final particles is isotropic in the center of mass (CM) frame. In other words, within this frame, it is assumed that the two final nucleons move in opposite directions with equal energy and opposite momentum, and the emission angles are randomly chosen in the CM, assuming an isotropic

Published by the American Physical Society under the terms of the [Creative Commons Attribution 4.0 International](https://creativecommons.org/licenses/by/4.0/) license. Further distribution of this work must maintain attribution to the author(s) and the published article's title, journal citation, and DOI. Funded by SCOAP³.

distribution. Once the final momenta are determined, a boost is applied to transition to the laboratory system, obtaining the momenta of the two ejected nucleons in this frame. Subsequently, these momenta are further propagated within a cascade FSI model [30,31].

Therefore, while these event generators employ theoretical or phenomenological methods to incorporate interactions during the propagation of the final state, it is crucial to recognize that the isotropic 2p distribution from which they begin is an assumption that may not be entirely accurate and could introduce uncertainties into the simulation results. The distinction between the isotropic distribution employed in MC generators and the more realistic distribution associated with a 2p2h microscopic model is primarily delineated by the value of the semi-inclusive hadronic tensor for a specific configuration of the two final particles. This crucial ingredient is absent in most current simulations. A recent endeavor to develop a microscopic model for calculating the distribution of two outgoing nucleons, when compared with the isotropic distribution model utilized in NEUT [32], has revealed significant discrepancies between the two distributions. This discrepancy between the isotropic assumption and the actual distribution of outgoing particles highlights a crucial area of interest in the study of neutrino-induced two-nucleon emission processes. It underscores the need for a more detailed and precise understanding of the semi-inclusive hadronic tensor within such processes, particularly with regard to the configurations of the final-state nucleons.

The relevance of studying semi-inclusive reactions and implementing them in Monte Carlo event generators is closely tied to the need for improving the reconstruction of incident neutrino energy based on measurements of the final state. This reconstruction would be possible if both the final leptonic and hadronic states were known. Efforts in this direction have included recent measurements of semi-inclusive observables, which involve the kinematics of both the final lepton and hadron(s), conducted by the T2K, MINERvA, and MicroBooNE Collaborations [33–37].

Simultaneously, a series of recent investigations have focused on the theoretical [38–40] study of semi-inclusive reactions induced by neutrinos, where one nucleon is detected in coincidence with the lepton [31,41–44]. However, the semi-inclusive one nucleon emission also has a contribution from 2p2h processes and, in general, multinucleon emission. In the absence of a semi-inclusive model for the 2p2h channel, attempts to estimate this contribution have modeled it using the Monte Carlo implementation of 2p2h in GENIE [43,44]. This, in turn, assumes that the distribution of two nucleons is isotropic in the center of mass, neglecting again the dependence of microscopical hadronic tensor on the semi-inclusive variables. Therefore, this shows that there is a need for theoretical studies of microscopic semi-inclusive versions associated with the 2p2h cross sections.

In this paper, we embark on an in-depth exploration of this issue. Our objective is to investigate the semi-inclusive cross section in two-particle emission reactions induced by neutrinos, employing a simple yet nontrivial microscopic model that consistently incorporates the 2p2h hadronic tensor. This endeavor will enable us to scrutinize the distribution of the

two final nucleons and elucidate how it deviates from the isotropic distribution in the CM frame. To achieve this, we utilize a relativistic model of electroweak MEC [45,46] in conjunction with the relativistic mean field (RMF) model of nuclear matter. [47–49].

The MEC 2p2h responses, calculated within the framework of the relativistic Fermi gas (RFG) model, have found extensive application in numerous analyses and calculations of inclusive neutrino and antineutrino cross sections, in conjunction with superscaling analysis (SuSA, SuSAv2) and the spectral function model [50–53], and have been implemented within the GENIE event generator as one of the widely utilized 2p2h parametrizations [29].

In the present work, we introduce several improvements to this 2p2h MEC model:

- (1) First we use the RMF framework, which accounts for the effects of the relativistic interaction between nucleons via scalar and vector potentials, giving rise to a relativistic effective mass and vector energy.
- (2) Second, we include the complete Δ propagator, encompassing both its real and imaginary parts. The Δ propagator assumes a crucial role within the MEC framework when a nucleon undergoes excitation to a Δ -isobar, subsequently decaying while interacting with a second nucleon. This process constitutes a fundamental component of the mechanisms underlying two-nucleon emission for high energy transfer.

The 2p2h MEC model, based on the RMF framework considered in this work has been employed to compute the inclusive 2p2h responses and cross sections in neutrino and antineutrino charged-current (CC) scattering [54–56]. This very model has also been recently utilized to analyze the interference between the one-body current and MEC contributions within the 1p1h response [57]. However, the primary focus of this work lies in exploring the semi-inclusive response associated with the emission of two particles, as deduced from this microscopic model. In the realm of semi-inclusive reactions, the two emitted nucleons possess known momenta in the proton-proton (PP), neutron-proton (NP), or neutron-neutron channels. Yet, the state of the residual nucleus remains unknown. One of the fundamental requirements for semi-inclusive distributions is that their integral equals the inclusive 2p2h cross section. This condition is essential to ensure the model's full consistency with the inclusive framework, and it constitutes one of the fundamental tests in this study.

The study of two-nucleon semi-inclusive reactions presents an additional challenge due to the fact that the distributions of two nucleons expand a six-dimensional space, making it impractical to visualize results for the full two-nucleon distribution. A commonly employed approach is to fix four or five of the final variables, either angles or momenta, and then examine the distributions in the remaining variables, typically one or two dimensions. However, this method may not yield general conclusions unless the complete map of configurations is explored, a task that is infeasible within the confines of a few pages. In this work, as it marks our initial exploration

of these observables, we present the results in an alternative manner. Our approach involves fixing one or two final variables and integrating over the remaining ones. This allows us to study partial semi-inclusive cross sections, of the onefold or twofold type. These onefold and twofold semi-inclusive cross sections encapsulate the global information of the full six-dimensional (6D) distribution, effectively averaging over the remaining variables. This approach simplifies the comparison between pure phase-space distributions and the model incorporating the hadronic tensor. Moreover, it allows for more straightforward conclusions to be drawn, as any differences observed in the onefold or twofold distributions imply corresponding differences in the overall distributions. By employing this strategy, we aim to provide a comprehensive view of the semi-inclusive reactions induced by neutrinos, shedding light on the intricacies of two-nucleon emission processes.

In Sec. II, we expound upon the formalism governing semi-inclusive and inclusive two-nucleon knockout processes initiated by neutrinos. In Sec. III, we delve into the method of calculation for both the onefold and twofold cross sections employed in this study. This method involves partial summations over bins within the space of exclusive variables. Section IV is devoted to the presentation of our results, which encompass a range of lepton kinematics relevant to neutrino scattering reactions. Finally, in Sec. V, we draw our conclusions, summarizing our findings and highlighting the key insights gleaned from this study.

II. FORMALISM

A. 2p2h cross section

In this paper we consider the reactions $(\nu_\mu, \mu^- N_1 N_2)$ and $(\bar{\nu}_\mu, \mu^+ N_1 N_2)$, where an incident (anti) neutrino with energy E_ν interact with a complex nucleus changing into a muon with kinetic energy T_μ and solid angle $\Omega_\mu = (\theta_\mu, \phi_\mu)$, with the result of the ejection of two nucleons, N_1, N_2 , with momenta $(\mathbf{p}'_1, \mathbf{p}'_2)$ in the final state plus a residual nucleus. The outgoing nucleons can be neutrons or protons, $N_i = N, P$. If the two nucleons are detected in coincidence with the μ^\pm lepton the probability of the reaction is determined by the semi-inclusive cross section

$$\frac{d\sigma_{N_1 N_2}}{dT_\mu d\Omega_\mu d^3 p'_1 d^3 p'_2} = \sigma_0(k, k') L_{\mu\nu} W_{N_1 N_2}^{\mu\nu}(\mathbf{p}'_1, \mathbf{p}'_2, \mathbf{q}, \omega), \quad (1)$$

where $L_{\mu\nu}$ is the leptonic tensor and $W_{N_1 N_2}^{\mu\nu}(\mathbf{p}'_1, \mathbf{p}'_2, \mathbf{q}, \omega)$ is the semi-inclusive hadronic tensor. Denoting the neutrino and muon four-momenta as $k^\nu = (\epsilon, \mathbf{k})$, and $k'^\nu = (\epsilon', \mathbf{k}')$, respectively, the momentum transfer is $\mathbf{q} = \mathbf{k} - \mathbf{k}'$ and the energy transfer is $\omega = \epsilon - \epsilon'$. The four-momentum transfer $Q^\mu = (\omega, \mathbf{q})$ verifies $Q^2 = \omega^2 - q^2 < 0$.

The function σ_0 in Eq. (1) is defined by

$$\sigma_0(k, k') = \frac{G^2 \cos^2 \theta_c}{4\pi^2} \frac{k'}{k}, \quad (2)$$

where $G = 1.166 \times 10^{-11} \text{ MeV}^{-2}$ is the Fermi constant, and θ_c is the Cabibbo angle, $\cos \theta_c = 0.975$.

The leptonic tensor $L_{\mu\nu}$ appearing in Eq. (1) is given by

$$L_{\mu\nu} = k_\mu k'_\nu + k_\nu k'_\mu - k k' g_{\mu\nu} \pm i \epsilon_{\mu\nu\alpha\beta} k^\alpha k'^\beta, \quad (3)$$

where $+$ ($-$) is for neutrino (antineutrino).

The semi-inclusive hadronic tensor $W_{N_1 N_2}^{\mu\nu}(\mathbf{p}'_1, \mathbf{p}'_2, \mathbf{q}, \omega)$ contains the information about the nuclear transition matrix elements of the weak current in the above reaction.

The inclusive cross section in the two-nucleon emission channel is recovered by integration over the two final nucleons

$$\begin{aligned} \left(\frac{d\sigma}{dT_\mu d\Omega_\mu} \right)_{2p2h} &= \sigma_0 L_{\mu\nu} \int d^3 p'_1 d^3 p'_2 W^{\mu\nu}(\mathbf{p}'_1, \mathbf{p}'_2, \mathbf{q}, \omega) \\ &= \sigma_0 L_{\mu\nu} W_{2p2h}^{\mu\nu}(\mathbf{q}, \omega), \end{aligned} \quad (4)$$

with

$$W^{\mu\nu}(\mathbf{p}'_1, \mathbf{p}'_2, \mathbf{q}, \omega) = \sum_{N_1 N_2} W_{N_1 N_2}^{\mu\nu}(\mathbf{p}'_1, \mathbf{p}'_2, \mathbf{q}, \omega), \quad (5)$$

where the isospin sum is performed over final pairs (NP, PP) in the case of neutrino scattering, and (NN, NP) for antineutrinos. The inclusive hadronic tensor in the two-particle, two-hole (2p2h) channel is defined as

$$W_{2p2h}^{\mu\nu}(\mathbf{q}, \omega) = \sum_{N_1 N_2} (W_{2p2h}^{\mu\nu})_{N_1 N_2}(\mathbf{q}, \omega), \quad (6)$$

where the inclusive 2p2h hadronic tensor in the (N_1, N_2) channel is

$$(W_{2p2h}^{\mu\nu})_{N_1 N_2}(\mathbf{q}, \omega) = \int d^3 p'_1 d^3 p'_2 W_{N_1 N_2}^{\mu\nu}(\mathbf{p}'_1, \mathbf{p}'_2, \mathbf{q}, \omega). \quad (7)$$

In Ref. [46] a MEC model was developed for the inclusive 2p2h hadronic tensor in the RFG. With independent-particle models such as the noninteracting Fermi gas, the emission of two particles in a nuclear transition is only possible through a two-body current operator. In this MEC model we consider the diagrams with exchange of a pion as shown in Fig. 1. This approach is based on the weak pion emission model of Ref. [58]. Here we consider the same MEC model extended [54] to include the RMF within the framework of the Walecka model [47–49]. In this model the inclusive 2p2h hadronic tensor in the N_1, N_2 channel is written

$$\begin{aligned} (W_{2p2h}^{\mu\nu})_{N_1 N_2} &= \frac{V}{(2\pi)^9} \int d^3 p'_1 d^3 p'_2 d^3 h_1 d^3 h_2 \frac{(m_N^*)^4}{E_1 E_2 E'_1 E'_2} \\ &\times w_{N_1 N_2}^{\mu\nu}(\mathbf{p}'_1, \mathbf{p}'_2, \mathbf{h}_1, \mathbf{h}_2) \delta(\mathbf{p}'_1 + \mathbf{p}'_2 - \mathbf{q} - \mathbf{h}_1 - \mathbf{h}_2) \\ &\times \theta(p'_1 - k_F) \theta(k_F - h_1) \theta(p'_2 - k_F) \theta(k_F - h_2) \\ &\times \delta(E'_1 + E'_2 - E_1 - E_2 - \omega), \end{aligned} \quad (8)$$

where $w_{N_1 N_2}^{\mu\nu}(\mathbf{p}'_1, \mathbf{p}'_2, \mathbf{h}_1, \mathbf{h}_2)$ is the elementary 2p2h hadronic tensor given below, Eq. (11), and $V/(2\pi)^3 = Z/(\frac{8}{3}\pi k_F^3)$ for symmetric nuclear matter with Fermi momentum k_F . In Eq. (8) the variable m_N^* is the relativistic effective mass of the nucleon, the four-momenta of the final particles and holes are $P_i'^\mu = (E'_i, \mathbf{p}'_i)$, and $H_i^\mu = (E_i, \mathbf{h}_i)$, respectively. Momentum conservation implies $\mathbf{p}'_2 = \mathbf{h}_1 + \mathbf{h}_2 + \mathbf{q} - \mathbf{p}'_1$.

Within the RMF model of nuclear matter [47–49], the nucleons are interacting with relativistic scalar and vector potentials, denoted $g_s \phi_0$ and $g_v V_0$, respectively, see Ref. [48].

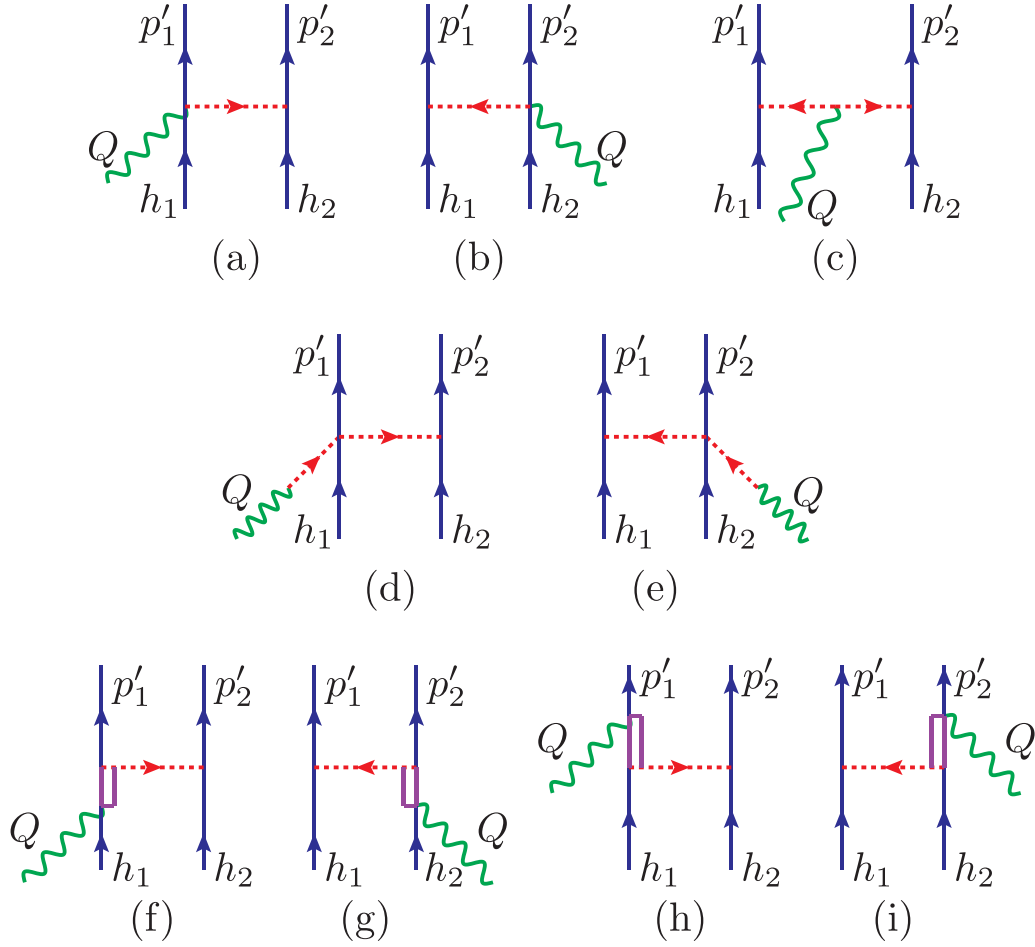


FIG. 1. Feynman diagrams of meson exchange currents considered in the present work.

The single-particle wave functions are plane waves with momentum \mathbf{p} , and with on-shell energy $E = [(m_N^*)^2 + p^2]^{1/2}$. The relativistic effective mass of the nucleon is defined by $m_N^* = m_N - g_s \phi_0 = M^* m_N$, where m_N is the free nucleon mass. Additionally the nucleon acquires a positive energy due to the repulsion by the relativistic vector potential, $E_v = g_v V_0$. Thus the total nucleon energy is $E_{RMF} = E + E_v$. Note that the vector energy does not appear explicitly in Eq. (8). This is because it cancels out by subtraction of particle and hole energies in the energy δ function. However it can be seen that the vector energy enters in the Δ current diagrams of Figs. 1(f)–1(i) through the energy of the intermediate Δ excitation (see Ref. [54] for details).

The nuclear states in the RMF are Slater determinants constructed with plane waves obtained by solving the free Dirac equation with effective mass m_N^* . Note that we use the same effective mass for particles and holes. All states with momentum $h < k_F$ are occupied in the ground state. The 2p2h excitations are obtained by raising two particles above the Fermi level, with momenta p'_1 and $p'_2 > k_F$, leaving two holes with momenta h_1 and $h_2 < k_F$. The 2p2h hadronic tensor is generated by the neutrino interaction with the two-body MEC operator, whose matrix elements can be

written as

$$\langle f | J^\mu(Q) | i \rangle = \frac{(2\pi)^3}{V^2} \delta(\mathbf{p}'_1 + \mathbf{p}'_2 - \mathbf{q} - \mathbf{h}_1 - \mathbf{h}_2) \times \frac{(m_N^*)^2}{\sqrt{E'_1 E'_2 E_1 E_2}} j^\mu(\mathbf{p}'_1, \mathbf{p}'_2, \mathbf{h}_1, \mathbf{h}_2). \quad (9)$$

The spin-isospin two-body current function $j^\mu(\mathbf{p}'_1, \mathbf{p}'_2, \mathbf{h}_1, \mathbf{h}_2)$ is the sum of diagrams of Fig. 1, described in detail in Refs. [46,54].

The elementary 2p2h hadronic tensor $w_{N_1 N_2}^{\mu\nu}(\mathbf{p}'_1, \mathbf{p}'_2, \mathbf{h}_1, \mathbf{h}_2)$, where N_1, N_2 are the charge states of the final nucleons, corresponds to the transition

$$| \mathbf{h}_1 s_1, \mathbf{h}_2 s_2 \rangle \rightarrow | \mathbf{p}'_1 s'_1, \mathbf{p}'_2 s'_2 \rangle, \quad (10)$$

where s_i, s'_j are the initial and final spin components. We denote this transition, in short, by $|1, 2\rangle \rightarrow |1', 2'\rangle$. Then the elementary 2p2h hadronic tensor is given by

$$w_{N_1 N_2}^{\mu\nu}(\mathbf{p}'_1, \mathbf{p}'_2, \mathbf{h}_1, \mathbf{h}_2) = \frac{1}{2} \sum_{s_1 s_2 s'_1 s'_2} j^\mu(1', 2', 1, 2)_A^* j^\nu(1', 2', 1, 2)_A, \quad (11)$$

where the two-body current matrix element is antisymmetrized with respect the pp or nn pair

$$j^\mu(1', 2', 1, 2)_A \equiv \begin{cases} j^\mu(1', 2', 1, 2) - j^\mu(1', 2', 2, 1) & \text{for } \nu_\mu NN \rightarrow \mu NP \quad \text{or } \bar{\nu}_\mu PP \rightarrow \mu^+ NP \\ j^\mu(1', 2', 1, 2) - j^\mu(2', 1', 1, 2) & \text{for } \nu_\mu NP \rightarrow \mu PP \quad \text{or } \bar{\nu}_\mu NP \rightarrow \mu^+ NN. \end{cases} \quad (12)$$

The factor 1/2 in Eq. (11) accounts for the antisymmetry of the two-body wave function with respect to exchange of momenta and spin quantum numbers to avoid double counting.

B. Probability distribution of 2p2h events

In this work we are interested in studying the probability distribution of semi-inclusive events corresponding to CC neutrino (antineutrino) scattering, $E_\nu \rightarrow (T_\mu, \Omega_\mu)$, with two outgoing nucleons N_1, N_2 with momenta $\mathbf{p}'_1, \mathbf{p}'_2$ in the final hadronic state. In Monte Carlo event generators the semi-inclusive event distribution is obtained by choosing two random momenta for the holes, $\mathbf{h}_1, \mathbf{h}_2$, below k_F . Then the total momentum and energy of the final nucleons is computed as $\mathbf{p}' = \mathbf{h}_1 + \mathbf{h}_2 + \mathbf{q}$ and $E' = E_1 + E_2 + \omega$. The individual momenta \mathbf{p}'_1 and \mathbf{p}'_2 for an event are generated by assuming an isotropic distribution of the two final nucleons in the CM frame, and then they are transformed to the Lab system. The 2p2h event $\mathcal{E} = (\mathbf{h}_1, \mathbf{h}_2, \mathbf{p}'_1, \mathbf{p}'_2)$ is allowed if the conditions $p'_i > k_F$ are verified. All 2p2h events \mathcal{E} of this kind that are allowed for a kinematics $(E_\nu, T_\mu, \Omega_\mu)$ contribute to the inclusive cross section with some probability that depends on the value of the hadronic tensor for the 2p2h event, $w^{\mu\nu}(\mathbf{p}'_1, \mathbf{p}'_2, \mathbf{h}_1, \mathbf{h}_2)$.

To find such probability within our MEC model we proceed as follows. We start with the inclusive 2p2h cross section written in the way

$$\frac{d\sigma_{N_1 N_2}}{dT_\mu d\Omega_\mu} = \frac{V}{(2\pi)^9} \int d^3 h_1 d^3 h_2 \theta(k_F - h_1) \theta(k_F - h_2) \times \frac{(m_N^*)^4}{E_1 E_2} F_{N_1 N_2}(\mathbf{h}_1, \mathbf{h}_2), \quad (13)$$

where the two-hole distribution function $F_{N_1 N_2}(\mathbf{h}_1, \mathbf{h}_2)$ determines the contribution of each pair of holes $(\mathbf{h}_1, \mathbf{h}_2)$. It is given by

$$F_{N_1 N_2}(\mathbf{h}_1, \mathbf{h}_2) = \int d^3 p'_1 d^3 p'_2 \frac{1}{E'_1 E'_2} \delta(E'_1 + E'_2 - E') \times \delta(\mathbf{p}'_1 + \mathbf{p}'_2 - \mathbf{p}') f_{N_1 N_2}(\mathbf{p}'_1, \mathbf{p}'_2, \mathbf{h}_1, \mathbf{h}_2), \quad (14)$$

where we have introduced the total energy and momentum in the final state, $E' = E_1 + E_2 + \omega$ and $\mathbf{p}' = \mathbf{h}_1 + \mathbf{h}_2 + \mathbf{q}$, respectively. The function $f_{N_1 N_2}(\mathbf{p}'_1, \mathbf{p}'_2, \mathbf{h}_1, \mathbf{h}_2)$ is

$$f_{N_1 N_2}(\mathbf{p}'_1, \mathbf{p}'_2, \mathbf{h}_1, \mathbf{h}_2) = \sigma_0 L_{\mu\nu} w_{N_1 N_2}^{\mu\nu}(\mathbf{p}'_1, \mathbf{p}'_2, \mathbf{h}_1, \mathbf{h}_2) \times \theta(p'_1 - k_F) \theta(p'_2 - k_F). \quad (15)$$

Note that $P'^\mu = (E', \mathbf{p}')$ is the total four-momentum of the two-particle final state $|\mathbf{p}'_1, \mathbf{p}'_2\rangle$ in the lab frame. The integral over $(\mathbf{p}'_1, \mathbf{p}'_2)$ in Eq. (14) can be performed by going to the center of mass system of the final nucleons. This was done in Ref. [59] to compute the 2p2h phase space in frozen approximation (for $\mathbf{h}_i = 0$). Here we extend the method to arbitrary

values of hole momenta and including the MEC dependence in the hadronic tensor.

Doubly primed variables refer to the CM system. The total final momentum in the CM is zero, $\mathbf{p}'' = \mathbf{p}''_1 + \mathbf{p}''_2 = 0$, and the total final energy E'' is determined by Lorentz invariance of the squared four-momentum, $E'' = (E'^2 - p'^2)^{1/2}$.

In the CM frame the two final nucleons are going back-to-back with the same momentum and with the same energy

$$E''_1 = E''_2 = \frac{E''}{2} = \frac{1}{2} \sqrt{E'^2 - p'^2} = \frac{1}{2} \sqrt{(E_1 + E_2 + \omega)^2 - (\mathbf{h}_1 + \mathbf{h}_2 + \mathbf{q})^2}. \quad (16)$$

The condition $E''_1 > m_N$ restricts the allowed values of $(\mathbf{h}_1, \mathbf{h}_2)$ for which two-nucleon emission is possible.

We perform the integration with respect CM coordinates, $\mathbf{p}'_1, \mathbf{p}'_2$, using $d^3 p'_i / E'_i = d^3 p''_i / E''_i$. Then we integrate over \mathbf{p}'_2 using the delta of momentum. The two-hole distribution function, Eq. (14), becomes

$$F_{N_1 N_2}(\mathbf{h}_1, \mathbf{h}_2) = \int d^3 p''_1 \frac{1}{(E''_1)^2} \delta(2E''_1 - E'') \times f_{N_1 N_2}(\mathbf{p}'_1, \mathbf{p}'_2, \mathbf{h}_1, \mathbf{h}_2) \theta(E'^2 - p'^2 - 4m_N^{*2}), \quad (17)$$

where $\mathbf{p}'_2 = -\mathbf{p}'_1$. The step function $\theta(E'^2 - p'^2 - 4m_N^{*2})$ ensures that the invariant mass of the final two-particle hadronic system is larger than $2m_N^*$ and also that the total speed of the CM is $v < 1$. Using $h'_i dh'_i = E''_i dE''_i$ to integrate over the energy, E''_1 with the help of the Dirac δ function, we obtain $E''_1 = E''/2$, as expected. This fixes the value of the modulus $p''_1 = [(E''/2)^2 - (m_N^*)^2]^{1/2}$, resulting in

$$F_{N_1 N_2}(\mathbf{h}_1, \mathbf{h}_2) = \frac{p''_1}{2E''_1} \int d\Omega''_1 f_{N_1 N_2}(\mathbf{p}'_1, \mathbf{p}'_2, \mathbf{h}_1, \mathbf{h}_2) \times \theta(E'^2 - p'^2 - 4m_N^{*2}), \quad (18)$$

where $d\Omega''_1 = d \cos \theta''_1 d\phi''_1$ are the angles of \mathbf{p}'_1 in the CM system. Note that the function $f_{N_1 N_2}(\mathbf{p}'_1, \mathbf{p}'_2, \mathbf{h}_1, \mathbf{h}_2)$ inside the integral (18) has to be evaluated for the momenta $\mathbf{p}'_1, \mathbf{p}'_2$ in the lab system. Then once $\mathbf{p}'_1, \mathbf{p}'_2$ are defined they are boosted back to the lab system.

The CM moves with velocity $\mathbf{v} = \mathbf{p}'/E'$. The direction of the velocity is defined by the unit vector $\mathbf{u} = \mathbf{v}/v$. The boost of a CM vector (E'', \mathbf{p}'') to the lab system can be written using $\gamma = 1/(1 - v^2)^{1/2}$:

$$p''_u = \gamma(vE'' + p''_u), \quad (19)$$

$$\mathbf{p}''_\perp = \mathbf{p}''_\perp, \quad (20)$$

where $p''_u = \mathbf{p}'' \cdot \mathbf{u}$ is the component along \mathbf{u} , and \mathbf{p}''_\perp is the invariant component perpendicular to \mathbf{u} . Using $\mathbf{p}' = p''_u \mathbf{u} + \mathbf{p}''_\perp$

we can write

$$\begin{aligned}\mathbf{p}' &= \gamma(vE'' + p''_u)\mathbf{u} + \mathbf{p}''_{\perp} \\ &= [\gamma vE'' + (\gamma - 1)p''_u]\mathbf{u} + p''_u\mathbf{u} + \mathbf{p}''_{\perp} \\ &= [\gamma vE'' + (\gamma - 1)p''_u]\mathbf{u} + \mathbf{p}''.\end{aligned}\quad (21)$$

Therefore the vectors \mathbf{p}'_i in the lab system inside the integral (18) can be computed as

$$\mathbf{p}'_i = [\gamma vE''_i + (\gamma - 1)p''_i \cdot \mathbf{u}]\mathbf{u} + \mathbf{p}''_{i\perp}.\quad (22)$$

Inserting Eq. (18) into (13) we can write the 2p2h inclusive cross section in the N_1N_2 channel as

$$\begin{aligned}\left(\frac{d\sigma_{N_1N_2}}{dT_{\mu}d\Omega_{\mu}}\right)_{2p2h} &= \frac{V}{(2\pi)^9} \int d^3h_1 d^3h_2 \theta(k_F - h_1) \theta(k_F - h_2) \\ &\quad \times \theta(E'^2 - p'^2 - 4m_N^{*2}) \\ &\quad \times \frac{(m_N^*)^4}{E_1 E_2} \frac{p''_1}{2E''_1} \int d\Omega''_1 f_{N_1N_2}(\mathbf{p}'_1, \mathbf{p}'_2, \mathbf{h}_1, \mathbf{h}_2).\end{aligned}\quad (23)$$

This integral over eight dimensions is computed using numerical methods. Note that with eight coordinates $(h_1, \theta_1, \phi_1, h_2, \theta_2, \phi_2, \theta_r, \phi_r)$, we generate the full space of exclusive events $\mathcal{E} = (\mathbf{h}_1, \mathbf{h}_2, \mathbf{p}'_1, \mathbf{p}'_2)$. For clarity here we denote by (θ_r, ϕ_r) the two nucleon angles relative to the CM, i.e.,

$$\theta_r = \theta''_1, \quad \phi_r = \phi''_1.\quad (24)$$

Thus the 2p2h inclusive cross section is finally written as

$$\begin{aligned}\left(\frac{d\sigma_{N_1N_2}}{dT_{\mu}d\Omega_{\mu}}\right)_{2p2h} &= \int_{S_F} d^3h_1 \int_{S_F} d^3h_2 \int d\cos\theta_r d\phi_r \\ &\quad \times G_{N_1N_2}(\mathbf{h}_1, \mathbf{h}_2, \theta_r, \phi_r),\end{aligned}\quad (25)$$

where the integrals over holes is performed in the Fermi sphere, S_F , that is, for $h_i < k_F$, and the function $G_{N_1N_2}$ is

$$\begin{aligned}G_{N_1N_2}(\mathbf{h}_1, \mathbf{h}_2, \theta_r, \phi_r) &= \frac{V}{(2\pi)^9} \frac{(m_N^*)^4}{E_1 E_2} \frac{p''_1}{2E''_1} \sigma_0 L_{\mu\nu} w_{N_1N_2}^{\mu\nu}(\mathbf{p}'_1, \mathbf{p}'_2, \mathbf{h}_1, \mathbf{h}_2) \\ &\quad \times \theta(p'_1 - k_F) \theta(p'_2 - k_F) \theta(E'^2 - p'^2 - 4m_N^{*2}),\end{aligned}\quad (26)$$

with

$$E' = E_1 + E_2 + \omega, \quad p' = |\mathbf{h}_1 + \mathbf{h}_2 + \mathbf{q}|,\quad (27)$$

and the factor

$$\frac{p''_1}{2E''_1} = \frac{1}{2} \sqrt{1 - \frac{4(m_N^*)^2}{(E_1 + E_2 + \omega)^2 - (\mathbf{h}_1 + \mathbf{h}_2 + \mathbf{q})^2}}\quad (28)$$

comes from the Jacobian of the Lorentz transformation to the CM system. Note that the step function $\theta(E'^2 - p'^2 - 4m_N^{*2})$ ensures that the value of above square root is real. The function $G_{N_1N_2}(\mathbf{h}_1, \mathbf{h}_2, \theta_r, \phi_r)$ determines the probability distribution of exclusive events.

C. Semi-inclusive 2p2h events

Starting from Eq. (25), the inclusive cross section can be calculated numerically. We proceed by a discretization

procedure by selecting a representative set of the exclusive events that contribute to the inclusive cross section. With this set of exclusive events all kinds of semi-inclusive events can be generated and computed through partial sums. We must clarify the difference between the concepts of exclusive event and semi-inclusive event in the context of this approach.

- (1) By *exclusive event* we mean a set of four-vectors $\mathcal{E} = (\mathbf{h}_1, \mathbf{h}_2, \mathbf{p}'_1, \mathbf{p}'_2)$ that represent a particular excitation of a 2p2h state that is compatible with conservation of energy and momentum, and thus contributes to the integral (25). Each exclusive event, in turn, can be expressed as a set of two hole momenta and two relative angles in the center-of-mass system of the final nucleons $\mathcal{E} = (\mathbf{h}_1, \mathbf{h}_2, \theta_r, \phi_r)$. Note that each exclusive event carries an implicit, fixed value of the moment and energy transfer \mathbf{q}, ω .
- (2) A *semi-inclusive event* refers to a fixed value of the final momenta $\mathcal{E}' = (\mathbf{p}'_1, \mathbf{p}'_2)$ without specifying values for the holes $(\mathbf{h}_1, \mathbf{h}_2)$, which are not observed. Therefore there are many pairs of nucleons, $(\mathbf{h}_1, \mathbf{h}_2)$, that can contribute to a given semi-inclusive event \mathcal{E}' , which implies in term of probability or cross section a sum (or integral) over the contributing pairs, $(\mathbf{h}_1, \mathbf{h}_2)$, with the given restriction that they belong to the semi-inclusive event \mathcal{E}' .
- (3) A *partial semi-inclusive event* is defined by specifying a subset of the six coordinates $(\mathbf{p}'_1, \mathbf{p}'_2)$ of the final state. In this work we consider (i) the *onefold events* that correspond to fixing one of the values $(p'_1, \theta'_1, \phi'_1, p'_2, \theta'_2, \phi'_2)$, and (ii) the *twofold events* that correspond to fixing two of them. This allows us to simplify the study of the semi-inclusive cross section, which depends on six variables, attacking first the simpler problem of the analysis of its partial integrals as will be seen below in more detail.
- (4) Finally, a *relative semi-inclusive event* refers to the specification of the two relative angles (θ_r, ϕ_r) of the final particles, in the CM system of the final nucleons. It must be clarified that in a relative event of this type the total momentum of the final nucleons is not constant because many pairs of initial nucleons $(\mathbf{h}_1, \mathbf{h}_2)$ can contribute, and therefore the relative semi-inclusive events are not observable. But it will be useful to analyze the distribution of these relative events in order to study the influence of the hadronic tensor on the semi-inclusive cross section.

The probability distribution of partial semi-inclusive events that we study in the next section is determined by the following onefold semi-inclusive cross sections:

$$\frac{d\sigma_{N_1N_2}}{dT_{\mu}d\Omega_{\mu}d p'_i}, \quad \frac{d\sigma_{N_1N_2}}{dT_{\mu}d\Omega_{\mu}d\cos\theta'_i}, \quad \frac{d\sigma_{N_1N_2}}{dT_{\mu}d\Omega_{\mu}d\phi'_i},\quad (29)$$

for $i = 1, 2$, obtained by integration of the sixfold semi-inclusive cross section over five final variables. For instance

$$\frac{d\sigma_{N_1N_2}}{dT_{\mu}d\Omega_{\mu}d p'_1} = \int p_1'^2 d\Omega_1' d^3 p_2' \frac{d\sigma_{N_1N_2}}{dT_{\mu}d\Omega_{\mu}d^3 p_1' d^3 p_2'}.\quad (30)$$

The twofold semi-inclusive cross sections are the following:

$$\frac{d\sigma_{N_1N_2}}{dT_\mu d\Omega_\mu d p'_1 d p'_2}, \quad \frac{d\sigma_{N_1N_2}}{dT_\mu d\Omega_\mu d \cos \theta'_1 d \cos \theta'_2},$$

$$\frac{d\sigma_{N_1N_2}}{dT_\mu d\Omega_\mu d \phi'_1 d \phi'_2}, \quad (31)$$

$$\frac{d\sigma_{N_1N_2}}{dT_\mu d\Omega_\mu d p'_i d \cos \theta'_j}, \quad \frac{d\sigma_{N_1N_2}}{dT_\mu d\Omega_\mu d p'_i d \phi'_j},$$

$$\frac{d\sigma_{N_1N_2}}{dT_\mu d\Omega_\mu d \cos \theta'_i d \phi'_j}. \quad (32)$$

with $i, j = 1, 2$.

We discretize the integration domain of Eq. (25) to generate a finite set of bins of exclusive events. We choose the integration variables $(h_1^3, \cos \theta_1, \phi_1, h_2^3, \cos \theta_2, \phi_2, \cos \theta_r, \phi_r)$. We divide the integration interval of each variable into a finite number of subintervals of respective widths $(\Delta h^3, \Delta \cos \theta, \Delta \phi, \Delta h^3, \Delta \cos \theta, \Delta \phi, \Delta \cos \theta_r, \Delta \phi_r)$. Note that we use the variable h^3 instead of h to perform the discretization, that goes from 0 to k_F^3 . This is convenient because the property $h^2 dh = dh^3/3$ to improve the precision in the numerical integral. We use the same integration widths for the two initial nucleons. In this way the space of exclusive events is discretized as a finite set $\{\mathcal{E}_i | i = 1, \dots, \mathcal{N}\}$. The volume element in the discretized space of exclusive events is

$$\Delta \mathcal{E} = \left(\frac{1}{3} \Delta h^3 \Delta \cos \theta_h \Delta \phi_h\right)^2 \Delta \cos \theta_r \Delta \phi_r. \quad (33)$$

The inclusive cross section can be approximated as a sum over discrete exclusive events

$$\left(\frac{d\sigma_{N_1N_2}}{dT_\mu d\Omega_\mu}\right)_{2p2h} \simeq \sum_{i=1}^{\mathcal{N}} G_{N_1N_2}(\mathcal{E}_i) \Delta \mathcal{E}. \quad (34)$$

In the limit $\Delta \mathcal{E} \rightarrow 0$ the exact cross section is obtained.

According to Eq. (34) the probability of each exclusive event, for a given lepton kinematics E_ν, T_μ, Ω_μ is given by

$$P_{N_1N_2}(\mathcal{E}) = \frac{G_{N_1N_2}(\mathcal{E}) \Delta \mathcal{E}}{\left(\frac{d\sigma_{N_1N_2}}{dT_\mu d\Omega_\mu}\right)_{2p2h}}, \quad (35)$$

and it is normalized to one:

$$\sum_{i=1}^{\mathcal{N}} P_{N_1N_2}(\mathcal{E}_i) = 1. \quad (36)$$

The function $G_{N_1N_2}(\mathcal{E})$ is given by Eq. (26) where we see that, for fixed values \mathbf{h}_1 and \mathbf{h}_2 , the outgoing nucleons are distributed according to the available phase space but they are *not* generated uniformly in the center of mass of the final hadronic system because the function $G_{N_1N_2}(\mathcal{E})$ depends on the value of the exclusive 2p2h hadronic tensor, $w^{\mu\nu}(\mathcal{E})$ for the event \mathcal{E} . This contrasts with the procedure used in most model implementations in neutrino interaction event generators, where an isotropic distribution for the two outgoing nucleons is assumed. This is the case, for instance, of the NUWRO [26], NEUT [32], and GENIE [29] event generators. Something similar happens in GiBUU implementation of the 2p2h excitations where the exclusive hadronic tensor does not

depend on the event \mathcal{E} [14]. In the results section we study the effect of including or not the exclusive hadronic tensor in the distribution of the final particles and the difference between the distributions in the different charge channels (PN, PP, or NN).

III. ONE- AND TWOFOLD 2p2h SEMI-INCLUSIVE CROSS SECTIONS

To calculate the one- and twofold semi-inclusive cross sections, we begin by generating the discrete set of exclusive events corresponding to a specific lepton kinematics. This means a uniform set of coordinates $(h_1^3, \cos \theta_1, \phi_1, h_2^3, \cos \theta_2, \phi_2, \cos \theta_r, \phi_r)$ for holes and relative angles of the particles, providing a discrete set of exclusive events \mathcal{E}_i that generates the inclusive cross section. In fact, the first check we make is that the sum over events of the function $G(\mathcal{E})$, Eq. (34), reproduces the inclusive 2p2h cross section for the given kinematics.

Discretization in the space of exclusive events implies in particular the discretization of semi-inclusive events $(\mathbf{p}'_1, \mathbf{p}'_2)$. We divide the intervals of possible values of the exclusive variables into n subintervals or *bins*:

$$p'_i : [k_F, (p'_i)_{\max}] = [p_i^{(1)}, p_i^{(2)}, \dots, p_i^{(n+1)}], \quad (37)$$

$$\cos \theta'_i : [-1, 1] = [\cos \theta_i^{(1)}, \cos \theta_i^{(2)}, \dots, \cos \theta_i^{(n+1)}], \quad (38)$$

$$\phi'_i : [0, 2\pi] = [\phi_i^{(1)}, \phi_i^{(2)}, \dots, \phi_i^{(n+1)}], \quad (39)$$

where the maximum momentum of final nucleons is $(p'_i)_{\max} = [(E'_i)_{\max}^2 - (m_N^*)^2]^{1/2}$ with $(E'_i)_{\max} = E_F + \omega$, corresponding to a nucleon with Fermi energy that receives all the energy transfer.

A. Onefold semi-inclusive cross sections

The onefold semi-inclusive cross sections can be computed for each bin as follows:

Let X be one of the semi-inclusive variables $X = p'_i, \cos \theta'_i, \phi'_i$, for $i = 1, 2$. For each exclusive event \mathcal{E} we denote by $X(\mathcal{E})$ the corresponding coordinate of the event. For instance if $\mathcal{E} = (\mathbf{h}_1, \mathbf{h}_2, \mathbf{p}'_1, \mathbf{p}'_2)$ is an event, then $p'_1(\mathcal{E}) = p'_1$. Let us now define by $B(X^{(k)})$ the subset of events \mathcal{E} such as $X^{(k)} \leq X(\mathcal{E}) < X^{(k+1)}$. That is, the event \mathcal{E} belong to the k th bin of the variable X , i.e., the interval $[X^{(k)}, X^{(k+1)})$

$$B(X^{(k)}) \equiv \{\mathcal{E} \text{ such that } X^{(k)} \leq X(\mathcal{E}) < X^{(k+1)}\}. \quad (40)$$

The total probability that an event belong to the bin k is obtained by summing the probabilities of all events that fall within the bin

$$P_{N_1N_2}(X^{(k)}) = \sum_{\mathcal{E} \in B(X^{(k)})} P_{N_1N_2}(\mathcal{E}), \quad (41)$$

verifying

$$\sum_k P_{N_1N_2}(X^{(k)}) = \sum_k \sum_{\mathcal{E} \in B(X^{(k)})} P_{N_1N_2}(\mathcal{E}) = 1. \quad (42)$$

Let be $\Delta X = X^{(k+1)} - X^{(k)}$ the (constant) width of the bin of the X variable. We define

$$S(X^{(k)}) = \frac{P_{N_1 N_2}(X^{(k)})}{\Delta X} \left(\frac{d\sigma_{N_1 N_2}}{dT_\mu d\Omega_\mu} \right)_{2p2h}. \quad (43)$$

Using Eq. (42) we obtain

$$\sum_k S(X^{(k)}) \Delta X = \left(\frac{d\sigma_{N_1 N_2}}{dT_\mu d\Omega_\mu} \right)_{2p2h}. \quad (44)$$

Therefore we identify $S(X^{(k)})$ as the corresponding onefold semi-inclusive cross section averaged over the bin $X^{(k)}$:

$$\left. \frac{d\sigma_{N_1 N_2}}{dT_\mu d\Omega_\mu dX} \right|_{X^{(k)}} = S(X^{(k)}) = \frac{1}{\Delta X} \sum_{\mathcal{E} \in B(X^{(k)})} G_{N_1 N_2}(\mathcal{E}) \Delta \mathcal{E}. \quad (45)$$

By summation over semi-inclusive bins we recover the inclusive 2p2h cross section,

$$\sum_k \left. \frac{d\sigma_{N_1 N_2}}{dT_\mu d\Omega_\mu dX} \right|_{X^{(k)}} \Delta X = \frac{d\sigma_{N_1 N_2}}{dT_\mu d\Omega_\mu}. \quad (46)$$

By this approach we compute the six onefold 2p2h semi-inclusive cross sections as

$$\left. \frac{d\sigma_{N_1 N_2}}{dT_\mu d\Omega_\mu dp'_i} \right|_{p_i^{(k)}} = \frac{1}{\Delta p'_i} \sum_{\mathcal{E} \in B(p_i^{(k)})} G_{N_1 N_2}(\mathcal{E}) \Delta \mathcal{E}, \quad (47)$$

$$\left. \frac{d\sigma_{N_1 N_2}}{dT_\mu d\Omega_\mu d \cos \theta'_i} \right|_{\cos \theta_i^{(k)}} = \frac{1}{\Delta \cos \theta'_i} \sum_{\mathcal{E} \in B(\cos \theta_i^{(k)})} G_{N_1 N_2}(\mathcal{E}) \Delta \mathcal{E}, \quad (48)$$

$$\left. \frac{d\sigma_{N_1 N_2}}{dT_\mu d\Omega_\mu d\phi'_i} \right|_{\phi_i^{(k)}} = \frac{1}{\Delta \phi'_i} \sum_{\mathcal{E} \in B(\phi_i^{(k)})} G_{N_1 N_2}(\mathcal{E}) \Delta \mathcal{E}, \quad (49)$$

where the partial sums are performed over the subset of events corresponding to the bins of p'_i , $\cos \theta'_i$ or ϕ'_i :

$$B(p_i^{(k)}) = \{\mathcal{E} \text{ such that } p_1^{(k)} \leq p_1(\mathcal{E}) < p_1^{(k+1)}\}, \quad (50)$$

$$B(\cos \theta_i^{(k)}) = \{\mathcal{E} \text{ such that } \cos \theta_1^{(k)} \leq \cos \theta_1(\mathcal{E}) < \cos \theta_1^{(k+1)}\}, \quad (51)$$

$$B(\phi_i^{(k)}) = \{\mathcal{E} \text{ such that } \phi_1^{(k)} \leq \phi_1(\mathcal{E}) < \phi_1^{(k+1)}\}. \quad (52)$$

B. Twofold semi-inclusive cross sections

The above procedure to obtain the onefold semi-inclusive cross sections is straightforwardly extended to the case of twofold semi-inclusive cross sections. If $X \neq Y$ is a pair of semi-inclusive variables $X, Y = p'_i, \cos \theta'_i, \phi'_i$, for $i = 1, 2$, we construct the subset $B(X^{(k)}, Y^{(l)})$ of exclusive events \mathcal{E} such that $X(\mathcal{E})$ is inside the k th bin of the variable X , and $Y(\mathcal{E})$ is inside the l th bin of the variable Y , i.e.,

$$B(X^{(k)}, Y^{(l)}) \equiv \{\mathcal{E} \mid X^{(k)} \leq X(\mathcal{E}) < X^{(k+1)} \text{ and } Y^{(l)} \leq Y(\mathcal{E}) < Y^{(l+1)}\}. \quad (53)$$

The total probability that an event belong to the bins (k, l) of variables (X, Y) is then

$$P_{N_1 N_2}(X^{(k)}, Y^{(l)}) = \sum_{\mathcal{E} \in B(X^{(k)}, Y^{(l)})} P_{N_1 N_2}(\mathcal{E}). \quad (54)$$

Again the total probability is one:

$$\sum_{kl} P_{N_1 N_2}(X^{(k)}, Y^{(l)}) = \sum_{kl} \sum_{\mathcal{E} \in B(X^{(k)}, Y^{(l)})} P_{N_1 N_2}(\mathcal{E}) = 1. \quad (55)$$

As in the previous section, we define

$$S(X^{(k)}, Y^{(l)}) = \frac{P_{N_1 N_2}(X^{(k)}, Y^{(l)})}{\Delta X \Delta Y} \left(\frac{d\sigma_{N_1 N_2}}{dT_\mu d\Omega_\mu} \right)_{2p2h}. \quad (56)$$

Using Eq. (55) we obtain

$$\sum_{kl} S(X^{(k)}, Y^{(l)}) \Delta X \Delta Y = \left(\frac{d\sigma_{N_1 N_2}}{dT_\mu d\Omega_\mu} \right)_{2p2h}. \quad (57)$$

Therefore we identify $S(X^{(k)}, Y^{(l)})$ as the corresponding twofold semi-inclusive cross section averaged over the bins $X^{(k)}, Y^{(l)}$

$$\begin{aligned} \left. \frac{d\sigma_{N_1 N_2}}{dT_\mu d\Omega_\mu dX dY} \right|_{X^{(k)}, Y^{(l)}} &= S(X^{(k)}, Y^{(l)}) \\ &= \frac{1}{\Delta X \Delta Y} \sum_{\mathcal{E} \in B(X^{(k)}, Y^{(l)})} G_{N_1 N_2}(\mathcal{E}) \Delta \mathcal{E}. \end{aligned} \quad (58)$$

Is easy to check that the summation over twofold semi-inclusive bins, gives again the inclusive 2p2h cross section

$$\sum_{kl} \left. \frac{d\sigma_{N_1 N_2}}{dT_\mu d\Omega_\mu dX dY} \right|_{X^{(k)}, Y^{(l)}} \Delta X \Delta Y = \frac{d\sigma_{N_1 N_2}}{dT_\mu d\Omega_\mu}. \quad (59)$$

Therefore the probability distribution of the twofold events is related to the twofold semi-inclusive cross section by

$$\left. \frac{d\sigma_{N_1 N_2}}{dT_\mu d\Omega_\mu dX dY} \right|_{X^{(k)}, Y^{(l)}} = \frac{P_{N_1 N_2}(X^{(k)}, Y^{(l)})}{\Delta X \Delta Y} \left(\frac{d\sigma_{N_1 N_2}}{dT_\mu d\Omega_\mu} \right)_{2p2h}. \quad (60)$$

Using Eq. (58), the twofold 2p2h semi-inclusive cross sections are computed as

$$\begin{aligned} \left. \frac{d\sigma_{N_1 N_2}}{dT_\mu d\Omega_\mu dp'_1 dp'_2} \right|_{p_i^{(k)}, p_j^{(l)}} &= \frac{1}{\Delta p'_1 \Delta p'_2} \sum_{\mathcal{E} \in B(p_i^{(k)}, p_j^{(l)})} G_{N_1 N_2}(\mathcal{E}) \Delta \mathcal{E}, \end{aligned} \quad (61)$$

$$\begin{aligned} \left. \frac{d\sigma_{N_1 N_2}}{dT_\mu d\Omega_\mu d \cos \theta'_1 d \cos \theta'_2} \right|_{\cos \theta_1^{(k)}, \cos \theta_2^{(l)}} &= \frac{1}{\Delta \cos \theta'_1 \Delta \cos \theta'_2} \sum_{\mathcal{E} \in B(\cos \theta_1^{(k)}, \cos \theta_2^{(l)})} G_{N_1 N_2}(\mathcal{E}) \Delta \mathcal{E}, \end{aligned} \quad (62)$$

TABLE I. Selected lepton kinematics studied in this work: neutrino energy, muon energy, scattering angle and the corresponding values of q , ω and also the angle θ_q between \mathbf{q} and the neutrino direction (z axis).

Kinematics	E_ν [MeV]	E_μ [MeV]	$\cos \theta_\mu$	θ_μ [deg]	q [MeV/c]	ω [MeV]	θ_q [deg]
1	950	600	0.85	31.79	545.42	350	34.78
2	700	600	0.85	31.79	368.77	100	57.53
3	800	300	0.05	87.13	834.49	500	19.64
4	400	300	0.05	87.13	477.07	100	36.00
5	700	200	-0.75	138.59	834.93	500	7.73
6	300	200	-0.75	138.59	441.85	100	14.72

variables, with integration being performed across the remaining ones.

As shown in the preceding section, the probability of such partial events is computed through a partial summation of exclusive event probabilities within a discretized framework. The semi-inclusive variables \mathbf{p}'_1 and \mathbf{p}'_2 will similarly be discretely binned.

For the sake of convenience, we further present the outcomes in terms of probabilities concerning the distributions of feasible events of both onefold and twofold nature, while maintaining a constant neutrino kinematic configuration. The corresponding onefold and twofold cross sections are directly proportional to these probabilities, with the proportionality factor being precisely the inclusive 2p2h cross section. This value, established for the lepton kinematics, is divided by the bin volume, as indicated in Eqs. (43) and (60). In this study, we not delve into averaging over the neutrino flux. Instead, we operate under the assumption of an incident neutrino possessing a predetermined energy, yielding a muon with certain energy and scattering angle.

We consider the six kinematics given in Table I. These kinematics have been chosen as follows. First of all we choose three scattering angles $\cos \theta_\mu = 0.85, 0.05$ and -0.75 corresponding to three angular bins from the MiniBooNE experiment. In Fig. 3 we plot the inclusive 2p2h cross section averaged with the neutrino flux against the muon energy, for the three given angles. The position of the maximum on this cross section is indicated with the arrows in each panel, that corresponds approximately to the energy of the muon in the kinematics of Table I. In each panel of Fig. 3 we also show the 2p2h cross section for two fixed neutrino energies. The value of the first neutrino energy in the green curves is chosen so that the position of the maximum of the cross section roughly coincides with that of the averaged cross section. This is indicated by long thin arrows. These neutrino energies corresponds to kinematics 1, 3, and 5 of Table I.

The value of the second neutrino energy in the blue curves of Fig. 3 is chosen such that $\omega = 100$ MeV at the maximum of the average cross section. This corresponds to the kinematics 2, 4, and 6 of Table I. A short thick arrow shows the contribution of this second neutrino energy to the cross section before averaging in the flux. These neutrino energies give a smaller contribution to the 2p2h cross section.

Once the lepton kinematics are defined, the lepton tensor can be immediately calculated with Eq. (3) taking into account that the leptonic vectors and momentum transfer in the

coordinate system of Fig. 2 are the following:

$$k^\mu = (E_\nu, \mathbf{k}) = (E_\nu, 0, 0, E_\nu), \quad (71)$$

$$k^\nu = (E_\mu, \mathbf{k}') = (E_\mu, k' \sin \theta_\mu, 0, k' \cos \theta_\mu), \quad (72)$$

$$\mathbf{q} = \mathbf{k} - \mathbf{k}' = (-k' \sin \theta_\mu, 0, E_\nu - k' \cos \theta_\mu). \quad (73)$$

As explained in the last section, for each kinematic we generate exclusive events in terms of six coordinates ($h_1^3, \cos \theta_1, \phi_1, h_2^3, \cos \theta_2, \phi_2$) for the two holes, and two relative angles ($\cos \theta_r, \phi_r$) for the final particles. We generate a number of 7^6 hole pairs and 200^2 pairs of relative angles. The total number of exclusive events, $\mathcal{E} = (\mathbf{h}_1, \mathbf{h}_2, \mathbf{p}'_1, \mathbf{p}'_2)$, generated in this way is $N_{\text{events}} = 4.71 \times 10^9$ for each one of the kinematics of Table I.

Now, for each exclusive event, \mathcal{E}_i , we compute the exclusive hadronic tensor $w_{N_1 N_2}^{\mu\nu}(\mathcal{E}_i)$ for PP and NP (NN and NP) ejection in the case of neutrino (antineutrino) scattering. After contraction with the leptonic tensor, we build the values of the function $G_{N_1 N_2}(\mathcal{E}_i)$ of Eq. (26) that determine the probability distribution of events and the semi-inclusive cross sections. We sum over the events included in the selected bins, and compute the corresponding onefold and twofold semi-inclusive cross sections averaged over the bin using the Eqs. (45) and (58). Dividing by the inclusive cross section, the probability distribution of partial semi-inclusive events is obtained.

In this work we are interested in comparing with the pure phase-space isotropic distribution of final-state nucleons in the hadronic center-of-mass frame, similar to what is done in the Monte Carlo implementations [26]. This is equivalent to neglecting the dependence of the hadronic tensor $W_{N_1 N_2}^{\mu\nu}(\mathcal{E})$ on the exclusive event \mathcal{E} . In our calculation we simply set

$$\sigma_0 L_{\mu\nu} W_{N_1 N_2}^{\mu\nu}(\mathcal{E}) = 1. \quad (74)$$

The resulting semi-inclusive event distribution is only due to the kinematics of 2p2h phase-space (PS) and does not depend on the current matrix elements. In this case the probability of exclusive events is computed similarly to Eq. (35):

$$P_{\text{P.S.}}(\mathcal{E}) = \frac{G_{\text{P.S.}}(\mathcal{E})}{\sum_{\mathcal{E}'} G_{\text{P.S.}}(\mathcal{E}')}, \quad (75)$$

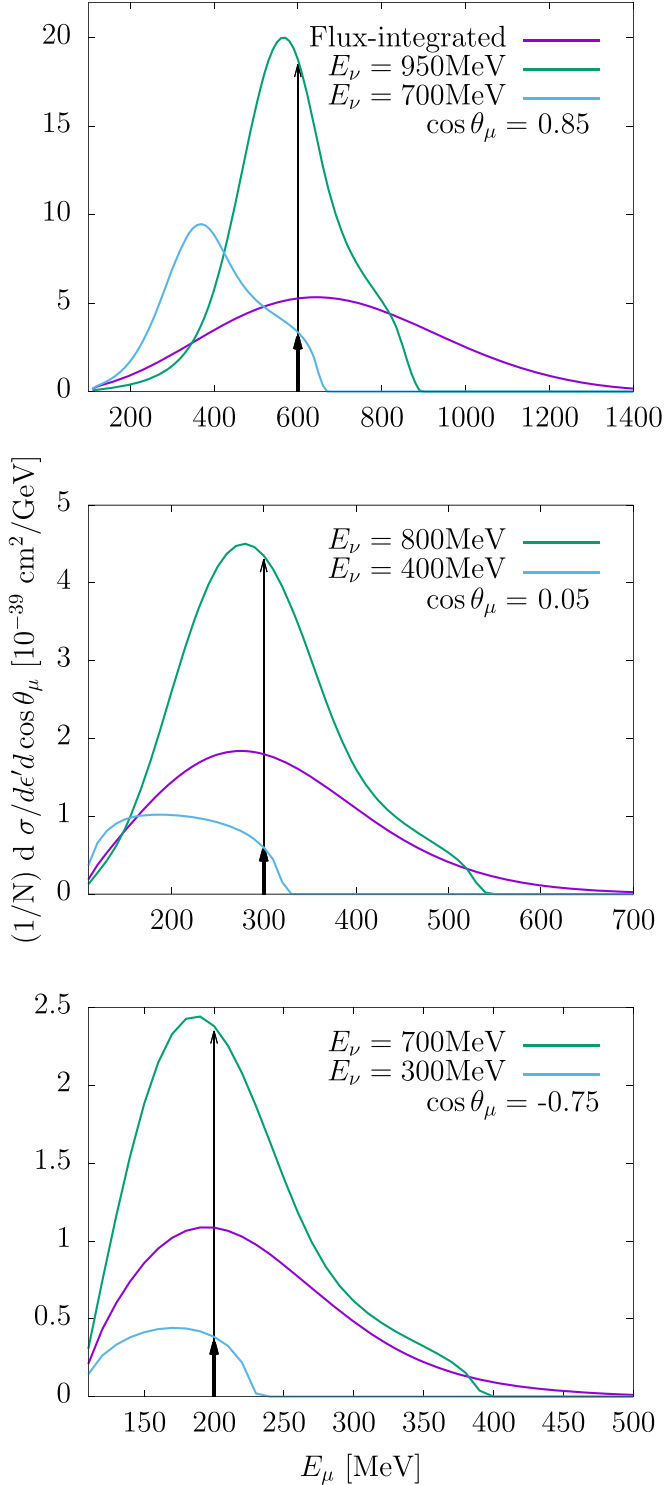


FIG. 3. Inclusive 2p2h neutrino cross section as a function of muon energy. Each panel corresponds to a fixed muon angle. In each panel we plot the cross section for two neutrino energies compared with the cross section averaged over the neutrino flux. The neutrino energies are those that appear in Table I. The arrows indicate the muon energies in the table.

where the exclusive phase-space $G_{\text{P.S.}}$ function is defined similarly to Eq. (26):

$$G_{\text{P.S.}}(\mathbf{h}_1, \mathbf{h}_2, \theta_r, \phi_r) = \frac{V}{(2\pi)^9} \frac{(m_N^*)^4}{E_1 E_2} \frac{p_1'}{2E_1'} \theta(p_1' - k_F) \times \theta(p_2' - k_F) \theta(E'^2 - p'^2 - 4m_N^{*2}). \quad (76)$$

Note that the $G_{\text{P.S.}}$ function does not depend on the charge of the nucleons, it only depends on the phase-space kinematics. Using this phase-space distribution we can define a semi-inclusive cross section whose integral is equal to the inclusive cross section, similarly to Eq. (77):

$$\frac{d\sigma_{\text{P.S.}}}{dT_\mu d\Omega_\mu dXdY} \Big|_{X^{(k)}, Y^{(l)}} \equiv \frac{P_{\text{P.S.}}(X^{(k)}, Y^{(l)})}{\Delta X \Delta Y} \left(\frac{d\sigma}{dT_\mu d\Omega_\mu} \right)_{2p2h}. \quad (77)$$

A. Twofold distributions

In Figs. 4 and 5 we show our results for the twofold semi-inclusive cross section of the relative angles in the center-of-mass system of the two outgoing nucleons, given by Eq. (69), for kinematics 1 and 2 of Table I. In the top panels we show the phase-space results. The NP and PP channels for neutrino scattering, $(\nu_\mu, \mu NP)$ and $(\nu_\mu, \mu PP)$, respectively, are also shown separately, as well as the NP and NN channels for antineutrino scattering, $(\bar{\nu}_\mu, \mu^+ NP)$, and $(\bar{\nu}_\mu, \mu^+ NN)$, respectively. All of them have been calculated including the full 2p2h hadronic tensor (11).

To begin our analysis, we first verified that the integrals of the distributions, as shown in Figs. 4 and 5 over the relative angles, yield the value of the inclusive 2p2h cross section for the specified kinematics and charge channel. This serves as a valuable test of our present calculation. In Refs. [54–56,60], inclusive 2p2h response functions were computed within a reference frame with the momentum transfer pointing along the z -axis, utilizing a seven-dimensional integration scheme. In contrast, in the present calculation the z -axis is aligned with the neutrino direction, necessitating an eight-dimensional integration. Moreover, we compute all components of the hadronic tensor, while in Refs. [54–56,60] only the inclusive response functions were calculated. This cross-check reinforces the consistency of our results.

In Figs. 4 and 5 the phase-space (PS) distributions are appropriately normalized to the total neutron-proton (NP) plus proton-proton (PP) inclusive neutrino cross section. A close inspection reveals that indeed, in the case of neutrino scattering, the sum of the NP and PP cross sections approximately matches the PS cross section in the upper panel. Furthermore, it is evident that the PP cross section is approximately seven times greater than the NP cross section. A similar value for the PP/NP ratio was reported in Ref. [61] around the Δ peak of the 2p2h inclusive response.

It is noteworthy that the NP and PP distributions differ from the phase-space distribution. This discrepancy arises from our inclusion of the exact dependence of the hadronic tensor on the exclusive variables of 2p2h excitations. It is noteworthy that the PS distribution is not perfectly uniform, primarily

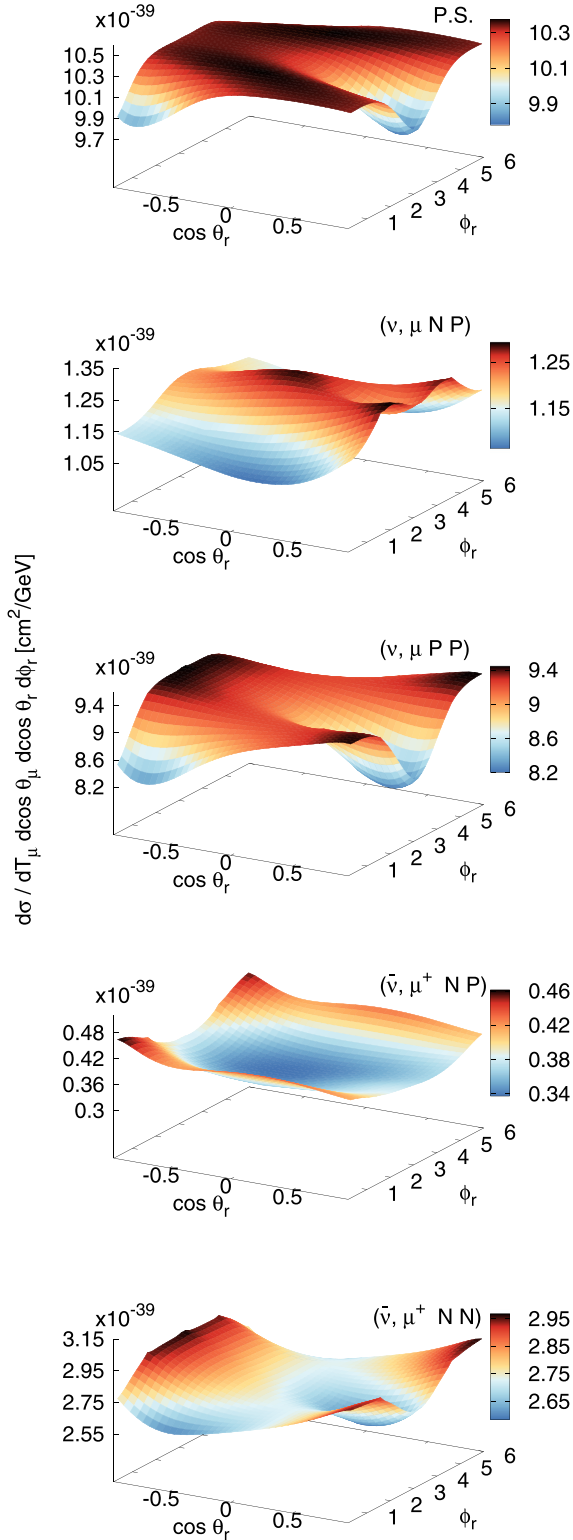


FIG. 4. Twofold Semi-inclusive cross section with respect to the relative angles in the center-of-mass system of the two outgoing nucleons. From top to bottom we show the phase-space, NP and PP emission with neutrinos, and NP and NN emission with antineutrinos. The kinematics is row 1 of Table I.

due to the summation over holes. Consequently, the center-of-mass momentum is not constant, resulting in an averaged

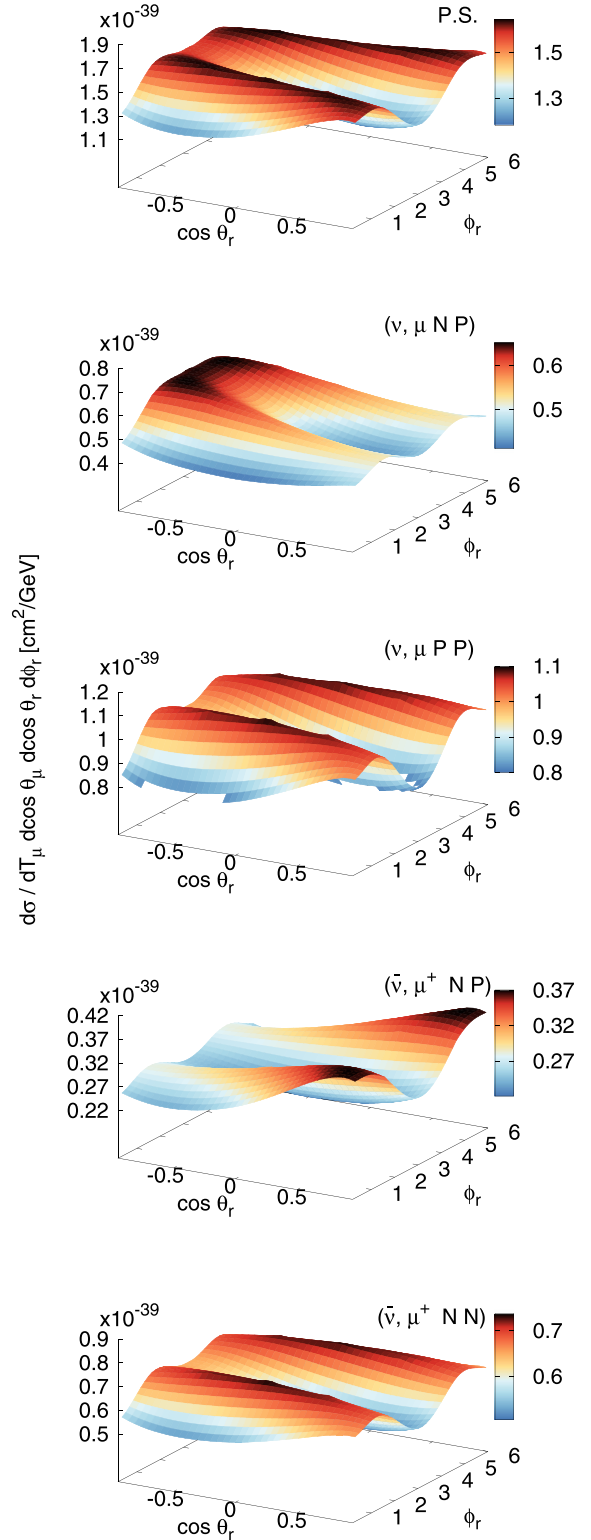


FIG. 5. The same as Fig. 4 for the kinematics row 2 of Table I.

distribution over all possible values of the center of mass contributing to the semi-inclusive observable. According to Table I, the results of Fig. 4 correspond to a neutrino energy $E_\nu = 950$ MeV, $q = 545$ MeV/ c and $\omega = 350$ MeV. For this case it is apparent that, according to phase space, the most

probable events cluster around the darker continuous band show in the top panel. However, a noticeable difference is observed compared with the neutrino PP and NP distributions, with the differences being more pronounced in the case of NP emission. Additionally, we note that the distribution peaks for NP and PP emission occur at different angles. In the case of antineutrinos, distinct distributions are also observed for NP and NN emissions, which deviate from the phase-space predictions. These observations emphasize the importance of considering the full dependence of the hadronic tensor on the exclusive variables.

The distributions of the relative angles also exhibit a significant dependence on the leptonic kinematics, as can be discerned when comparing them with the case of different kinematics, as exemplified in Fig. 5. In this scenario, characterized by a neutrino energy of 700 MeV, momentum transfer $q = 369$ MeV/ c and energy transfer $\omega = 100$ MeV, notable distinctions become apparent. In the case of neutrino scattering, the PP distribution closely aligns with the pure phase space, a feature corroborated by the location of the darker region where the cross section is larger. Conversely, the NP distribution deviates considerably from both the phase space and the PP distribution, with its maximum found at backward angles (θ_r). In this instance, the NP cross section is slightly smaller than that of the PP, although it remains of the same order of magnitude.

Similar trends are observed in the case of antineutrino scattering in Fig. 5. Turning our attention to the antineutrino NN cross section, it closely resembles the phase-space distribution, whereas the NP cross section exhibits noticeable differences. In this case, the maximum is shifted towards forward angles in θ_r . These nuanced variations underscore the intricacies of the semi-inclusive reactions and emphasize the impact of the hadronic tensor and lepton kinematics on the semi-inclusive 2p2h cross section.

The results presented in Figs. 4 and 5 are expressed in terms of absolute cross-section values. We have observed similar trends, demonstrating deviations of the semi-inclusive distributions from those expected for pure phase space, for all the leptonic kinematics of Table I. Notably, these differences are most pronounced for PN emission. These results provide a partial integration of the total semi-inclusive cross section. To gain a broader view of the entire six-dimensional landscape but in two-dimensional averaged sections, we now display results for the twofold cross sections involving pairs of the observable semi-inclusive variables ($p'_i, \cos \theta_i, \phi_i$). In this context, it is less critical to ascertain the absolute value of the cross section, as we are aware that the normalization is uniform across all distributions, with the inclusive cross section serving as a common reference for a given kinematic scenario. Therefore, we present the results in terms of probabilities for each semi-inclusive bin, understanding that the summation over bins in these distributions equals one. Our primary objective is to examine the differences among various semi-inclusive charge channels and their distinctions relative to a pure phase-space distribution.

We show a more complete example of the available twofold distributions in Figs. 6–8. In the interest of brevity and due to space limitations, we have chosen to focus on rep-

resentative examples of these combinations, mindful of not overwhelming the reader with an exhaustive display of every possible distribution. It is essential to acknowledge that illustrating every conceivable combination is impractical within the confines of this presentation. However, the selected distributions provide a meaningful and insightful glimpse into the complex multidimensional landscape of semi-inclusive reactions initiated by neutrinos and antineutrinos. Together, these figures provide a comprehensive perspective on the distributions within the semi-inclusive charge channels, enabling a deeper understanding of the deviations from pure phase-space models.

As a first example, in Fig. 6 we present the twofold distributions, namely, $P(p'_1, p'_2)$, $P(\cos \theta'_1, \cos \theta'_2)$, and $P(\phi'_1, \phi'_2)$, for both neutrino and antineutrino scattering. These distributions provide insights into the joint probability distributions of pairs of momenta or emission angles of the two particles within the semi-inclusive reactions. This example vividly demonstrates the correlations between pairs of variables and the differences introduced by considering the semi-inclusive hadronic tensor in contrast with pure phase-space distributions. Notably, these distributions show the asymmetries present in the final-state momenta of protons and neutrons within the NP channel, underscoring the influence of the hadronic tensor.

Specifically, the $P(p'_1, p'_2)$ distribution (first column of Fig. 6) reveals a strong correlation between these two variables. The distribution occupies a narrow band around a curve centered at (k_F, k_F) , corresponding to the minimum values the outgoing particles can attain. The global shape of the distribution is primarily dictated by kinematics, and does not depend on the hadronic tensor. We observe that the distribution is centered and exhibits a maximum around emission momenta of $p'_1 = p'_2 \approx 550$ MeV/ c for PP, NN, and the phase-space (PS) distributions. However, the NP distribution reveals a distinct pattern. For neutrino scattering, its maximum is centered approximately at $p'_1 \approx 650$ MeV/ c and $p'_2 = 450$ MeV/ c , while for antineutrino scattering, the situation is reversed, bearing in mind that particle 1 is a neutron and particle 2 is a proton. This clear asymmetry underscores the dissimilarity in final proton and neutron momenta within the NP channel, a consequence of the influence of the hadronic tensor.

In the second column of Fig. 6, we turn our attention to the correlations between the emission angles θ'_1 and θ'_2 . Here we also observe a distinctive pattern: the emission angles tend to cluster within a relatively narrow band, forming a curve that traverses from backward-forward $(-1, 1)$ to forward-backward $(1, -1)$ emissions. Within this band, all pairs of angles exhibit fairly similar probabilities, except in the extremes. Additionally, asymmetries in the distributions of NP emission concerning particles 1 and 2 are observed, even though they might not be as evident in the graph. Meanwhile, the distributions for PP, NN, and PS exhibit clear symmetry under the $1 \leftrightarrow 2$ exchange.

In the third column of Fig. 6, we finally explore the correlations between the azimuthal emission angles ϕ'_1 and ϕ'_2 , which correspond to the angles between the emission plane and the scattering plane (as illustrated in Fig. 2). Once again, we observe a distinct correlation shape that traces two

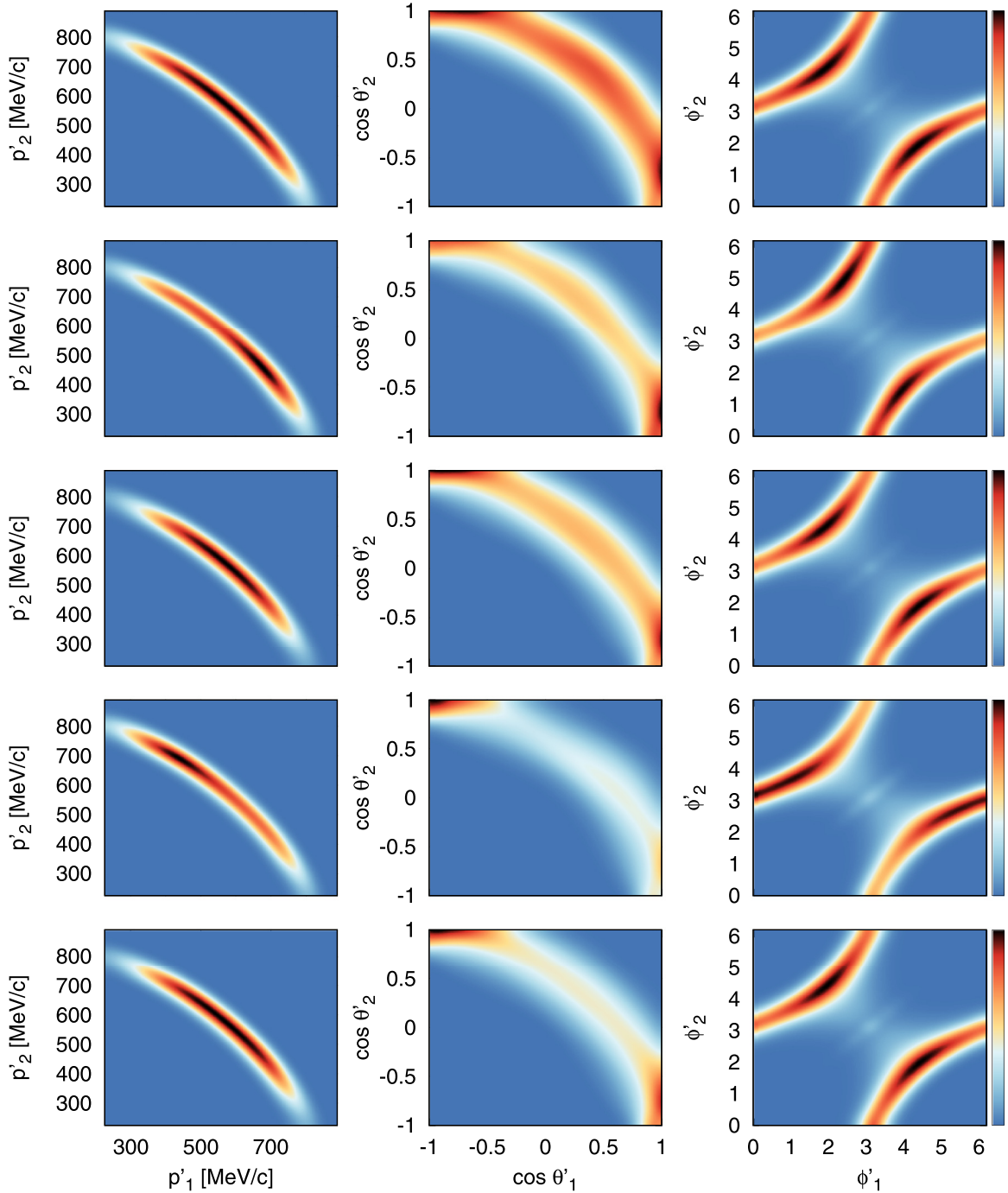


FIG. 6. Twofold distributions, namely, $P(p_1, p_2)$, $P(\cos \theta_1, \cos \theta_2)$, and $P(\phi_1, \phi_2)$, for kinematics row 1. From top to bottom we show the phase space, the neutrino NP and PP, and the antineutrino NP and NN emission channels, respectively. The units in each panel are such that the corresponding distribution is normalized to one.

precise trajectories in the (ϕ_1, ϕ_2) plane, ranging from $(0, \pi)$ to $(\pi, 2\pi)$ and from $(\pi, 0)$ to $(2\pi, \pi)$. It is worth noting that, in spherical coordinates, the values 0π and 2π are identified as the same point, so these two trajectories actually form a single path. In this case, we observe a clear $1 \leftrightarrow 2$ symmetry in the distributions for PP, NN, and the phase space around the angles of $(\pi/2, 3\pi/2)$ and $(3\pi/2, \pi/2)$. However, in the case of NP emission, this symmetry is disrupted again due to the influence of the hadronic tensor.

As a second example, depicted in Fig. 7, we present the twofold distributions $P(p'_1, \cos \theta'_1)$, $P(p'_1, \phi'_1)$, $P(p'_1, \cos \theta'_2)$, and $P(p'_1, \phi'_2)$, specifically for neutrino scattering and kinematics 1. These distributions shed light on the correlations between momentum of the first particle and one of the four angular variables. When comparing the phase-space, NP, and PP distributions, it is observed that they share a similar shape. This similarity is attributed to the fact that, as in the previous cases, the overall features are largely determined by

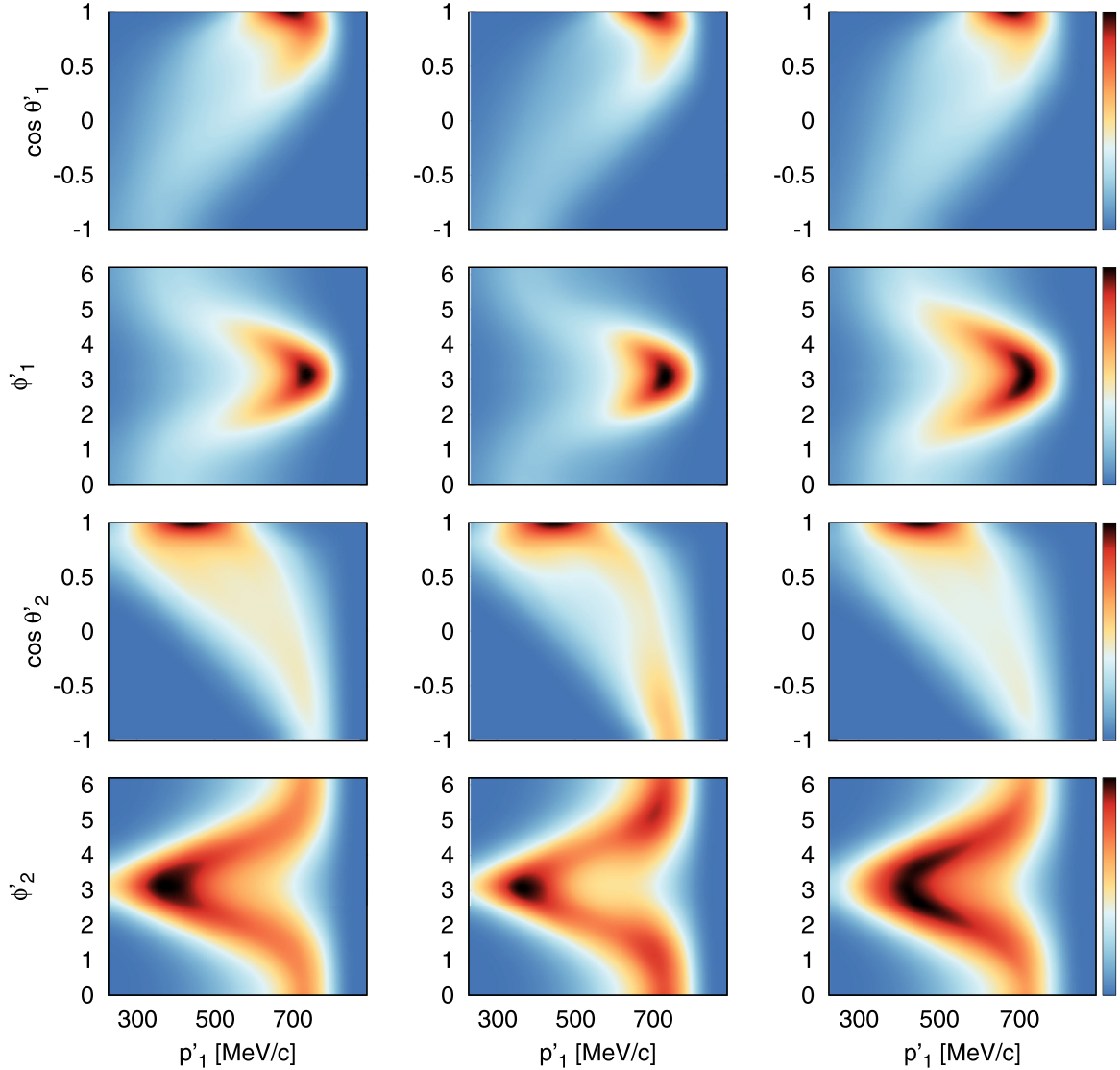


FIG. 7. Twofold distributions, $P(p_1, \cos \theta_1)$, $P(p_1, \phi_1)$, $P(p_1, \cos \theta_2)$, and $P(p_1, \phi_2)$, specifically for neutrino scattering and kinematics 1. In each panel from left to right we show the phase space, NP, and PP distributions.

kinematics, specifically energy and momentum conservation. The influence of the hadronic tensor alters the finer details, and clear differences can be observed between NP and PP emissions when compared with the phase-space distribution.

In a final example, in Fig. 8, we showcase the twofold distributions, $P(\cos \theta'_1, \phi'_1)$ and $P(\cos \theta'_1, \phi'_2)$, for neutrino scattering and kinematics 1, highlighting the joint probabilities associated with the emission angle of particle one and one of the azimuthal angles in the semi-inclusive reaction. Once more, we observe that the overall shapes of these distributions are similar among the three cases: phase-space, NP, and PP emissions. However, notable differences become evident in the detailed behavior of $P(\cos \theta'_1, \phi'_1)$, indicating that this distribution is particularly sensitive to the influence of the hadronic tensor. The distribution of $\cos \theta'_1$ and ϕ'_2 exhibits a pronounced peak around forward emission, and it becomes smoother away from that region. While there are still differences between the various

emission channels, these differences are not very noticeable in the figure.

To conclude the discussion of twofold distributions in semi-inclusive two-nucleon emission, Fig. 9 provides a comprehensive comparison of the distribution $P(p'_1, p'_2)$. This comparison covers kinematics 2 to 6 (rows in Fig. 9) for neutrino scattering, as outlined in Table I. The three columns, from left to right, correspond to phase-space, NP, and PP distributions, respectively. In this analysis, a clear correlation between the two momenta remains evident across all cases. In the instances of phase-space and PP emissions, the distributions exhibit clear symmetry with respect to $1 \leftrightarrow 2$ exchange. Then p'_1 equals p'_2 at the maximum of the distribution. Conversely, the NP distribution displays a clear asymmetry under $1 \leftrightarrow 2$ exchange, and $p'_1 \neq p'_2$ at the maximum. These results suggest that it is more likely for the neutron to possess more energy than the proton. The consistent trend of distinct distributions of momentum pairs between the NP and PP channels

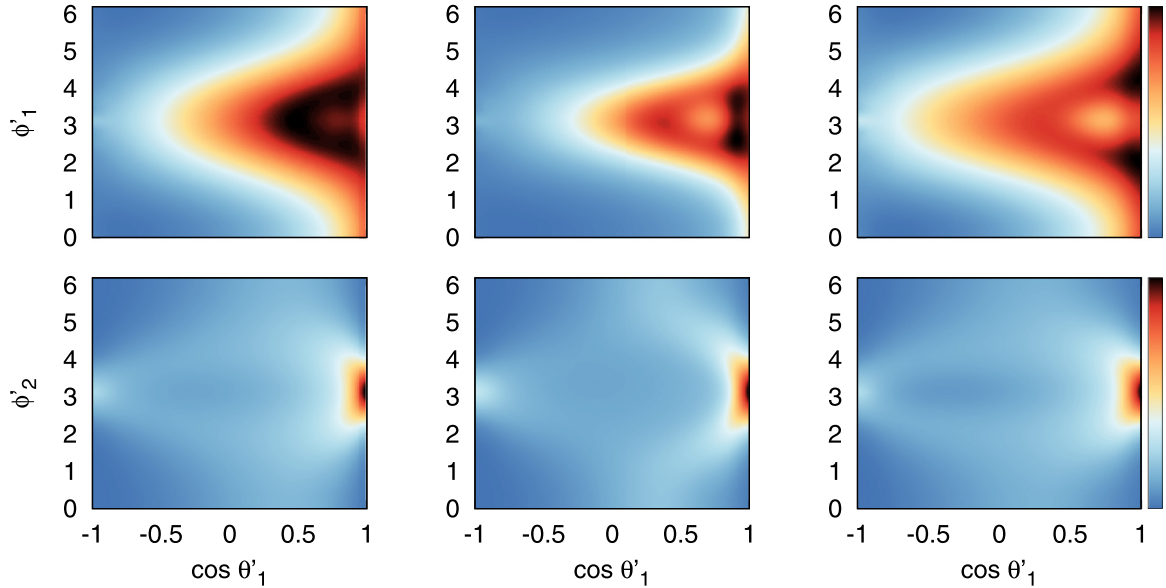


FIG. 8. Twofold semi-inclusive distributions, $P(\cos \theta'_1, \phi'_1)$ and $P(\cos \theta'_1, \phi'_2)$, for neutrino scattering and for kinematics 1. From left to right we show the phase-space, NP, and PP emission channels, respectively.

is observed across all the kinematic configurations analyzed in this study. This consistency underscores the necessity of including the hadronic tensor to accurately account for these differences.

B. Onefold distributions

Now we discuss the results for the onefold distributions in semi-inclusive two-nucleon emission induced by neutrinos (antineutrinos). Note that these onefold cross sections also contribute to semi-inclusive one-nucleon emission when combined with the results obtained from a model of one-nucleon knockout.

In Fig. 10, we present the distributions specifically for neutrino scattering, focusing on kinematics 1 as outlined in Table I. In each panel, we display the onefold distributions of the variables p'_1 , p'_2 , $\cos \theta'_1$, $\cos \theta'_2$, ϕ'_1 , ϕ'_2 as well as the angles in the center-of-mass (CM) frame of the final particles, $\cos \theta_r$ and ϕ_r . Within each panel, we provide a comparison between the distributions for phase-space (PS), NP, and PP channels.

In these distributions we fix the bins for one variable and integrate with respect to all other variables (or sum over all remaining bins). As a consequence the onefold distributions on the different channels appears quite similar. This is, in a way, an averaging effect on the hadronic tensor. However, despite this overall similarity, the NP channel exhibits notable distinctions from the NP and PP channels. The differences between the phase space and the two emission channels are typically on the order of 10%–20% depending on the kinematics.

We observe, when comparing the two top panels, that the distribution $P(p'_1)$ is equal to the $P(p'_2)$ distribution for PP emission. This equality arises due to the symmetry under the exchange of two protons. The same symmetry holds for the phase space, but in this case, it is because, by definition, the phase-space distribution depends solely on kinematics.

However, in the case of NP emission, this symmetry is not observed due to the inherent differences between the two outgoing particles and the isospin dependence of the hadronic tensor. Recall that particle 1 is a neutron and particle 2 is a proton. Consequently, the neutron distribution exhibits a more pronounced peak at higher momenta compared with the proton distribution.

Moving on to the panels of the second row in Fig. 10, we examine the distributions with respect to the polar emission angles, $P(\cos \theta'_1)$ and $P(\cos \theta'_2)$. Ideally, these two distributions should be exactly equal for the phase space, but in the figure, they do not appear exactly identical one being slightly higher than the other. This small discrepancy results from the numerical error introduced when discretizing the integrals into bins and the calculation method not treating particles 1 and 2 symmetrically. Consequently, the differences between these curves provide an estimate of the numerical error incurred when calculating these angular distributions, which here is approximately 5%. To reduce this error, one would need to decrease the bin size accordingly. However, this would significantly increase the number of exclusive events that need to be summed (and computed). It is important to keep this error in mind when interpreting the results of this study. Looking at the probability distributions in the panels of the second row, we notice that they increase with $\cos \theta'_1$, which means they decrease with the angle itself. This indicates that forward emission (with forward being the direction of the neutrino) is more probable, while backward emission is less likely.

Now we examine the two panels of the third row in Fig. 10 that display the distributions over the azimuthal angles. This indicates the probability of the orientation of the reaction plane of particle one with respect to the scattering plane when the other emerges in any direction, or vice versa in the case of particle 2. We observe that the prevailing trend is to be emitted predominantly in the semiplane with an angle of π , which is where the momentum transfer vector is contained

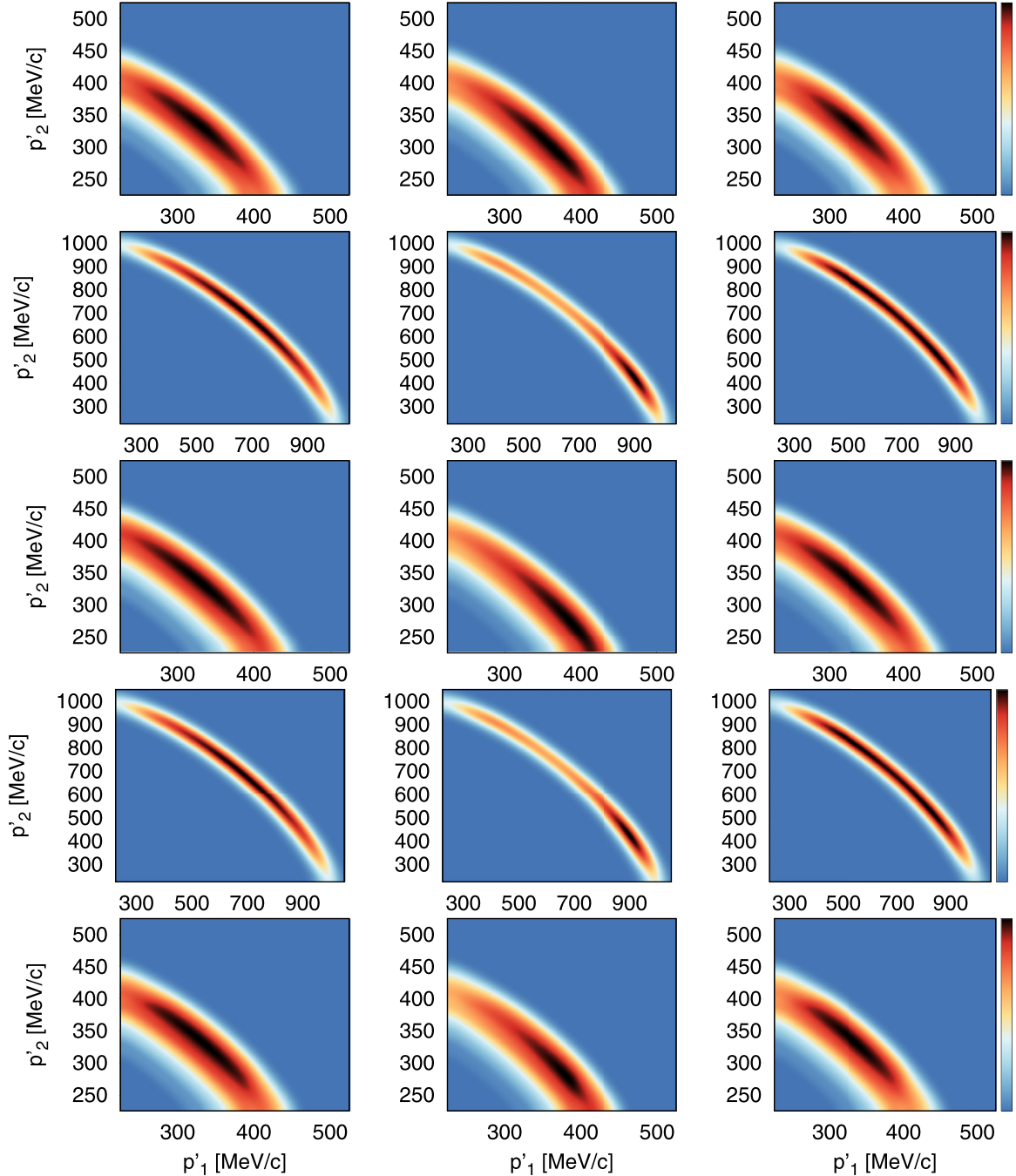


FIG. 9. Twofold distribution $P(p'_1, p'_2)$ for semi-inclusive 2p2h neutrino scattering. From top to bottom, the rows refer to the kinematics 2–6 of Table I, from left to right, the columns refer to the phase-space, NP, and PP distribution, respectively.

(see Fig. 2). There is an asymmetry in the case of NP emission when switching particle 1 for particle 2. This results in the neutron (particle 1) having a greater tendency to be emitted in the π plane (and adjacent planes) than the proton (particle 2).

Let us now examine the distributions with respect to the emission angles in the CM of the two final particles, shown in the bottom panels of Fig. 10. The distribution of $\cos\theta_r$ is quite flat in the case of phase space and PP emission, indicating that PP emission is approximately consistent with an isotropic distribution in the center of mass. However, it is also evident that NP emission is not as compatible with

this hypothesis, as the angular distribution deviates from the phase-space distribution. It is larger for forward angles and smaller for other angles.

In the case of the distribution of the relative azimuthal angle ϕ_r , both the PP and NP channels deviate from a pure isotropic distribution in the CM. The NP channel stands out as distinctly different from the other two. In this case, both the distributions for the PS and PP channels exhibit two maxima around $\pi/2$ and $3\pi/2$, with a minimum at π . In contrast, the NP distribution displays two larger maxima that are closer to π .

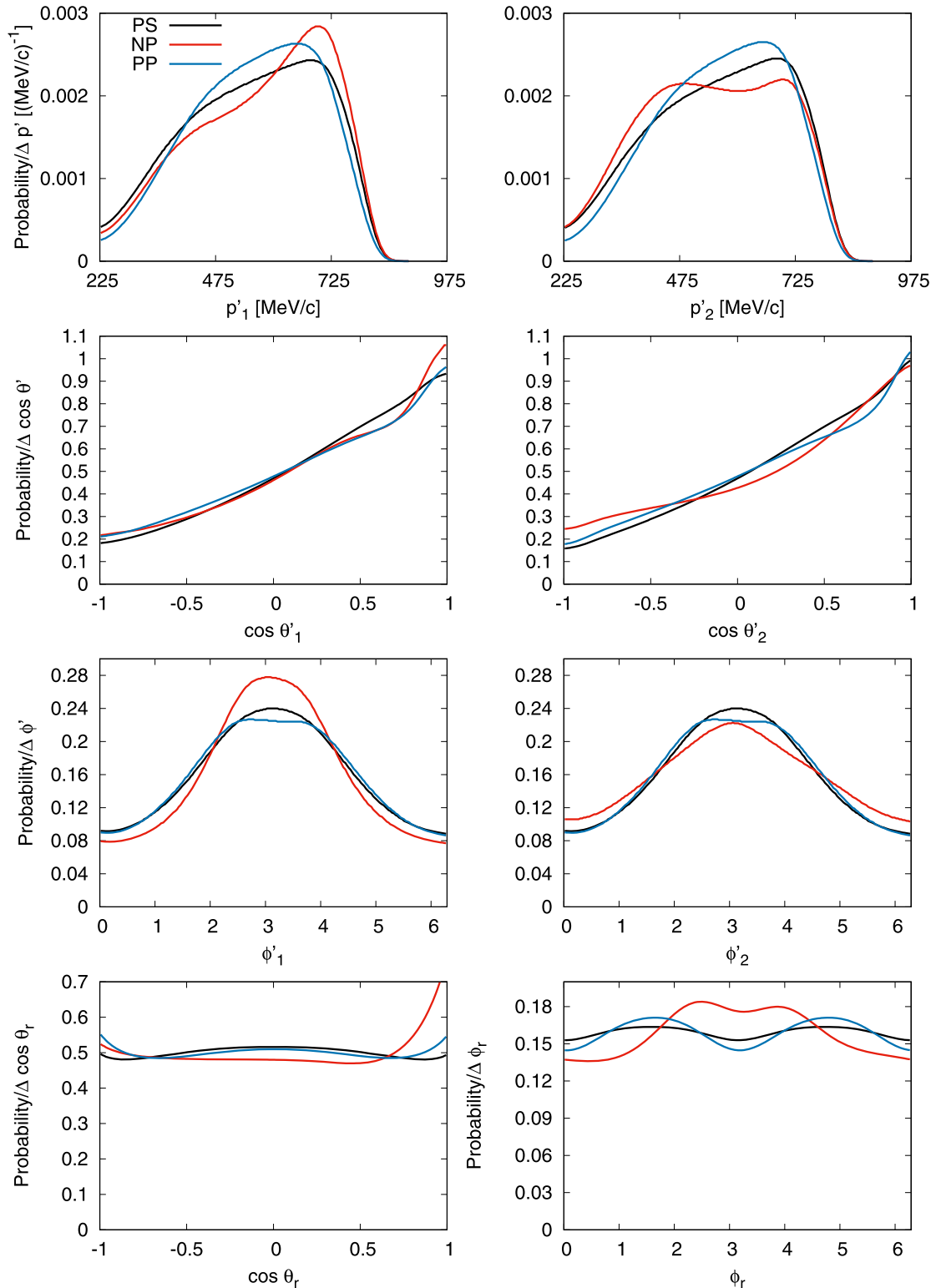


FIG. 10. Onefold distributions for semi-inclusive two-nucleon emission induced by neutrinos for kinematics 1. In each panel, we compare the distributions for phase-space (PS), NP, and PP emissions.

Similar differences are observed in Fig. 11, which corresponds to kinematics 2. However, comparing with Fig. 10, it becomes evident that the specific shape of the distribution also whimsically depends on the leptonic kinematics. Nonetheless, in almost all cases, the distributions in the case of NP

emission are notably different from the case of PP emission. To complete this discussion, we present in Figs. 12 and 13 results for antineutrino scattering for kinematics 1 and 2, to be compared with the corresponding Figs. 10 and 11 for neutrinos. They show similar trends, with the most noticeable

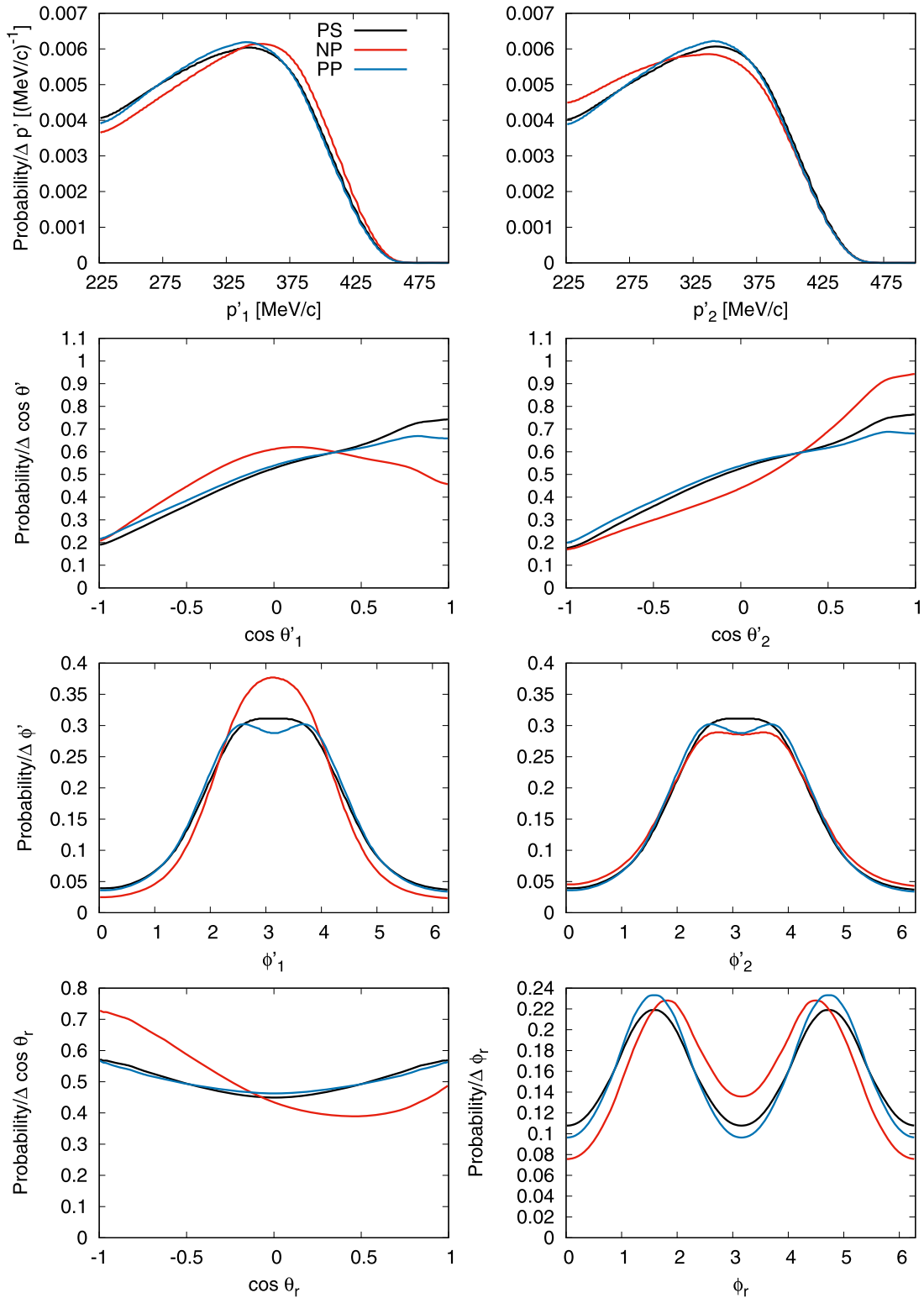


FIG. 11. The same of Fig. 10 for kinematics 2.

differences occurring again for NP emission as compared with the NN emission and the phase-space distribution, which are more similar. The most notable differences between NP and the others are observed in the distributions with respect to the azimuthal angles.

In any case, it is notable that the significant differences introduced by the hadronic tensor in the twofold distributions concerning relative angles, as shown in Figs. 4 and 5, tend to smooth out when we transition to distributions of the observable variables related to the momenta of the two nucleons.

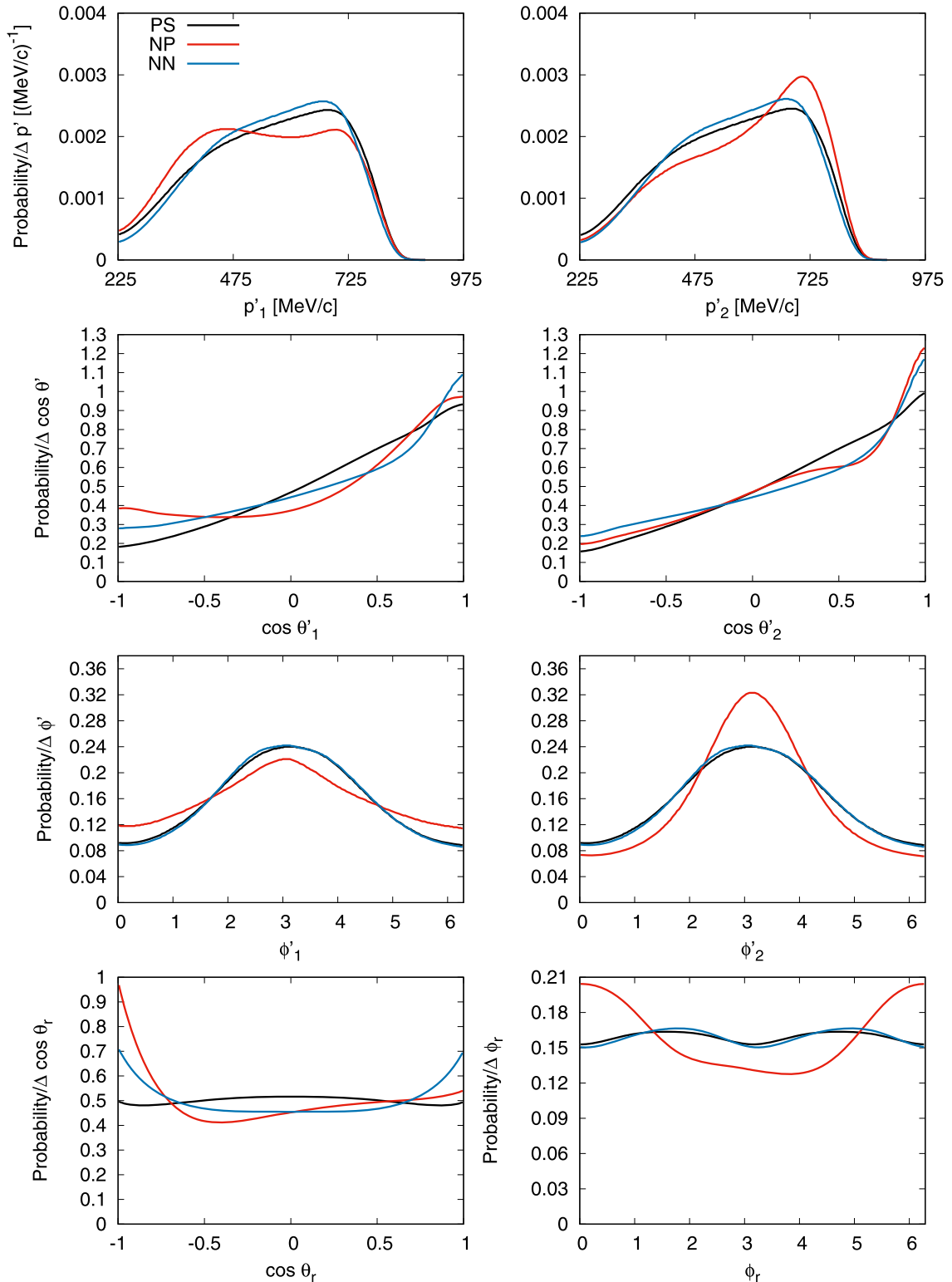


FIG. 12. Onefold distributions for semi-inclusive two-nucleon emission induced by antineutrinos for kinematics 1. In each panel, we compare the distributions for phase-space (PS), NP, and NN emission.

In other words, the very pronounced differences arising from considering different emission channels compared with the isotropic distribution in phase space seem to lessen when we consider the physical variables as a result of an average over

bins. It is expected that these differences become much more pronounced when considering the complete sixfold distribution, where the full impact of the hadronic tensor should be more prominent.

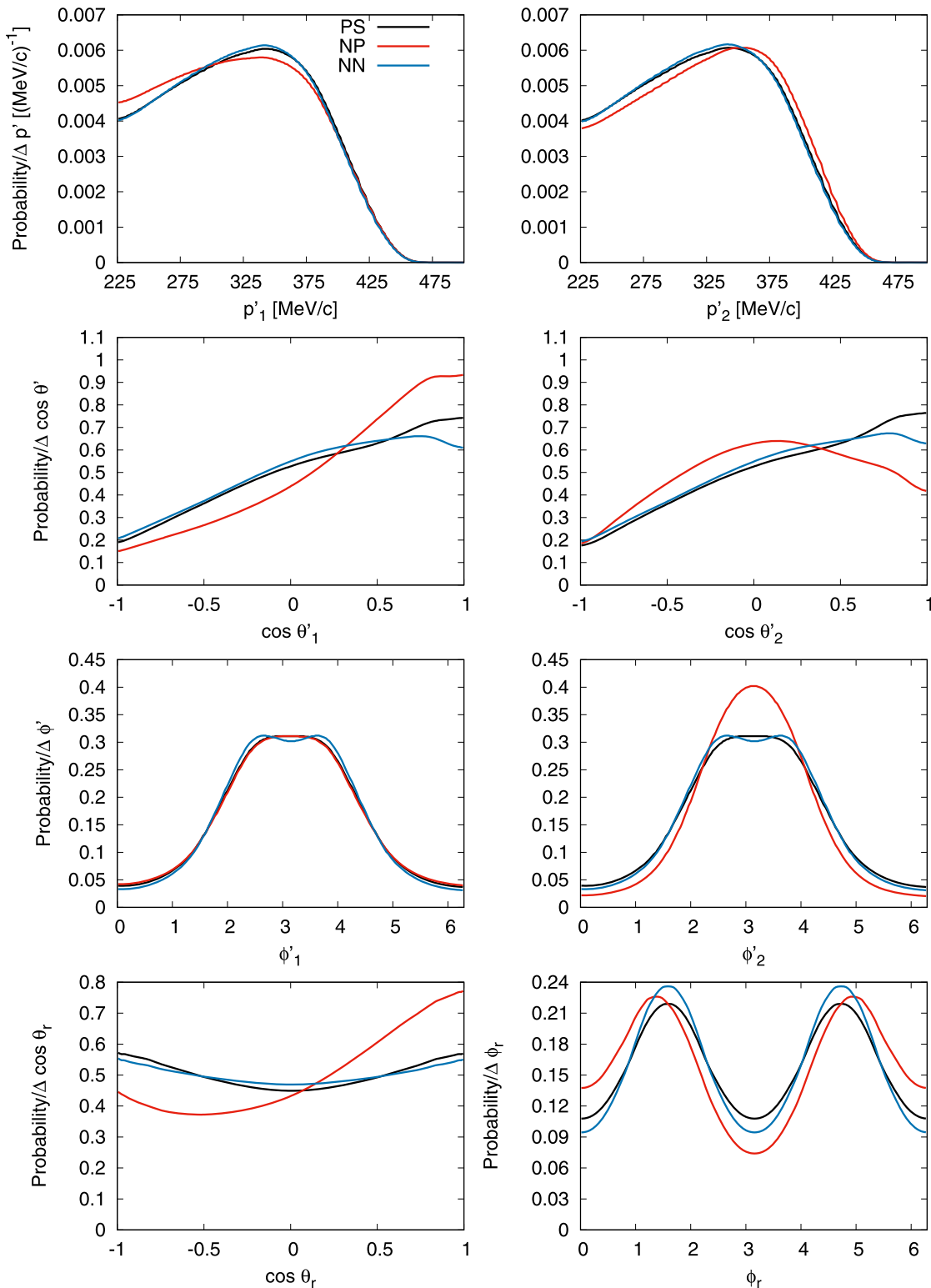


FIG. 13. The same as Fig. 12 but for kinematics 2.

V. CONCLUSIONS

In this work, we have undertaken a comprehensive study of the semi-inclusive cross section for two-nucleon emission induced by neutrinos and antineutrinos within a RMF model

of nuclear matter, including MEC. The primary aim of this study was to assess the differences between various emission channels, namely NP, PP, and NN, and to compare them with the pure phase-space model commonly employed in neutrino Monte Carlo event generators.

The novelty in this work lies in the inclusion of the full semi-inclusive hadronic tensor, derived from a microscopic calculation, whose integral recovers the inclusive 2p2h hadronic tensor. Given the complexity of a detailed study of the full six-dimensional distribution dependent on the final nucleon momenta, involving numerous variables, we conducted this preliminary investigation focusing on partial distributions dependent on only one or two variables (onefold and twofold distributions). We integrated over the remaining variables to gain insights into how the differences imposed by the hadronic tensor propagate through these observables, for various lepton kinematics.

Our findings reveal significant variations between the different emission channels, especially when compared with the pure phase-space model. These differences are particularly pronounced in distributions involving the relative angles in the CM frame. This is evidence that the isotropic distribution in the center of mass undergoes significant modifications when the hadronic tensor is included, effectively making it nonisotropic. This is particularly relevant in the case of NP emission, which seems to be related to the fact that the NP cross section is smaller than the PP cross section and is thus more sensitive to the influence of the hadronic tensor.

In the case of twofold distributions involving variables of the two emitted particles, the differences with the pure phase-space model are smaller due to the averaging effect of integrating over the remaining variables, which smoothes out the differences. Furthermore, these distributions are largely determined by kinematics, as energy and momentum conservation plays a significant role, and the hadronic tensor mainly influences the finer details of each distribution without altering the fundamental kinematic constraints.

From our results, we have observed strong correlations between pairs of variables (p'_1, p'_2), (θ'_1, θ'_2), and (ϕ'_1, ϕ'_2), which is evident from the corresponding twofold distributions.

When considering other combinations of two variables, there is generally very little correlation between them.

Appreciable differences are observed between the NP and PP distributions when the hadronic tensor is included in neutrino scattering. One notable result is that when an NP pair is emitted with neutrinos, it is more likely for the neutron to carry more energy than the proton, whereas the opposite is true for antineutrino scattering.

We have also presented results for the onefold distributions, which were obtained by fixing one semi-inclusive variable and integrating over the remaining ones. These distributions undergo relatively few variations when the hadronic tensor is included, primarily due to the smoothing effect of integration. Nevertheless, significant differences are observed between the cases of NP and PP emission, for neutrino scattering, and NP and NN emission, for antineutrino scattering, depending on the kinematics.

In conclusion, this work has explored semi-inclusive two-nucleon emission reactions induced by neutrinos, considering a microscopic treatment of the corresponding hadronic tensor. We have emphasized the differences with respect to the approach that assumes an isotropic distribution of the outgoing nucleons in the center of mass. This research is expected to be valuable for analyses based on Monte Carlo event generators and offers the potential for improving the reconstruction of incident neutrino energies. Future work could extend this study to the full six-dimensional distribution, providing even deeper insights into the impact of the hadronic tensor on these processes.

ACKNOWLEDGMENTS

The work was supported by Grant No. PID2020-114767GB-I00 funded by MCIN/AEI/10.13039/501100011033; and by Grant No. FQM-225 funded by Junta de Andalucía.

-
- [1] H. Gallagher, G. Garvey, and G. P. Zeller, *Annu. Rev. Nucl. Part. Sci.* **61**, 355 (2011).
- [2] J. G. Morfin, J. Nieves, and J. T. Sobczyk, *Adv. High Energy Phys.* **2012**, 934597 (2012).
- [3] J. A. Formaggio and G. P. Zeller, *Rev. Mod. Phys.* **84**, 1307 (2012).
- [4] L. Alvarez-Ruso, Y. Hayato, and J. Nieves, *New J. Phys.* **16**, 075015 (2014).
- [5] U. Mosel, *Annu. Rev. Nucl. Part. Sci.* **66**, 171 (2016).
- [6] M. Sajjad Athar, A. Fatima and S. K. Singh, *Prog. Part. Nucl. Phys.* **129**, 104019 (2023).
- [7] A. Aguilar-Arevalo *et al.* (MiniBooNE Collaboration), *Phys. Rev. D* **81**, 092005 (2010).
- [8] A. Aguilar-Arevalo *et al.* (MiniBooNE Collaboration), *Phys. Rev. D* **88**, 032001 (2013).
- [9] G. A. Fiorentini *et al.* (MINERvA Collaboration), *Phys. Rev. Lett.* **111**, 022502 (2013).
- [10] K. Abe *et al.* (T2K Collaboration), *Phys. Rev. D* **87**, 092003 (2013).
- [11] M. Martini, M. Ericson, G. Chanfray, and J. Marteau, *Phys. Rev. C* **80**, 065501 (2009).
- [12] J. Nieves, I. R. Simo, and M. J. Vicente Vacas, *Phys. Rev. C* **83**, 045501 (2011).
- [13] J. E. Amaro, M. B. Barbaro, J. A. Caballero, T. W. Donnelly, and C. F. Williamson, *Phys. Lett. B* **696**, 151 (2011).
- [14] O. Lalakulich, K. Gallmeister, and U. Mosel, *Phys. Rev. C* **86**, 014614 (2012); **90**, 029902(E) (2014).
- [15] T. Van Cuyck, N. Jachowicz, R. Gonzalez-Jimenez, M. Martini, V. Pandey, J. Ryckebusch, and N. Van Dessel, *Phys. Rev. C* **94**, 024611 (2016).
- [16] T. Van Cuyck, N. Jachowicz, R. Gonzalez-Jimenez, J. Ryckebusch, and N. Van Dessel, *Phys. Rev. C* **95**, 054611 (2017).
- [17] E. B. Martinez, A. Mariano, and C. Barbero, *Phys. Rev. C* **103**, 015503 (2021).
- [18] A. Lovato, S. Gandolfi, J. Carlson, S. C. Pieper, and R. Schiavilla, *Phys. Rev. C* **91**, 062501(R) (2015).
- [19] A. Lovato, J. Carlson, S. Gandolfi, N. Rocco, and R. Schiavilla, *Phys. Rev. X* **10**, 031068 (2020).
- [20] N. Rocco, C. Barbieri, O. Benhar, A. De Pace, and A. Lovato, *Phys. Rev. C* **99**, 025502 (2019).

- [21] R. Gran, J. Nieves, F. Sanchez, and M. J. Vicente Vacas, *Phys. Rev. D* **88**, 113007 (2013).
- [22] M. Martini and M. Ericson, *Phys. Rev. C* **87**, 065501 (2013).
- [23] M. Martini and M. Ericson, *Phys. Rev. C* **90**, 025501 (2014).
- [24] J. E. Amaro, M. B. Barbaro, J. A. Caballero, and T. W. Donnelly, *Phys. Rev. Lett.* **108**, 152501 (2012).
- [25] J. M. Campbell *et al.*, [arXiv:2203.11110](https://arxiv.org/abs/2203.11110).
- [26] J. T. Sobczyk, *Phys. Rev. C* **86**, 015504 (2012).
- [27] C. Andreopoulos, A. Bell, D. Bhattacharya, F. Cavanna, J. Dobson, S. Dytman, H. Gallagher P. Guzowski *et al.*, *Nucl. Instrum. Methods Phys. Res., Sect. A* **614**, 87 (2010).
- [28] T. Katori, *AIP Conf. Proc.* **1663**, 030001 (2015).
- [29] S. Dolan, G. D. Megias, and S. Bolognesi, *Phys. Rev. D* **101**, 033003 (2020).
- [30] S. Dytman, Y. Hayato, R. Raboanary, J. T. Sobczyk, J. Tena-Vidal and N. Vololoniaina, *Phys. Rev. D* **104**, 053006 (2021).
- [31] J. M. Franco-Patino, R. Gonzalez-Jimenez, S. Dolan, M. B. Barbaro, J. A. Caballero, G. D. Megias, and J. M. Udias, *Phys. Rev. D* **106**, 113005 (2022).
- [32] J. E. Sobczyk, J. Nieves, and F. Sanchez, *Phys. Rev. C* **102**, 024601 (2020).
- [33] K. Abe *et al.* (The T2K Collaboration), *Phys. Rev. D* **98**, 032003 (2018).
- [34] X. G. Lu *et al.* (MINERvA Collaboration), *Phys. Rev. Lett.* **121**, 022504 (2018).
- [35] T. Cai *et al.* (MINERvA Collaboration), *Phys. Rev. D* **101**, 092001 (2020).
- [36] P. Abratenko *et al.* (MicroBooNE Collaboration), *Phys. Rev. D* **102**, 112013 (2020).
- [37] P. Abratenko *et al.* (MicroBooNE Collaboration), *Phys. Rev. Lett.* **125**, 201803 (2020).
- [38] O. Moreno, T. W. Donnelly, J. W. Van Orden, and W. P. Ford, *Phys. Rev. D* **90**, 013014 (2014).
- [39] J. W. Van Orden and T. W. Donnelly, *Phys. Rev. C* **100**, 044620 (2019).
- [40] J. M. Franco-Patino, J. Gonzalez-Rosa, J. A. Caballero, and M. B. Barbaro, *Phys. Rev. C* **102**, 064626 (2020).
- [41] J. M. Franco-Patino, M. B. Barbaro, J. A. Caballero, and G. D. Megias, *Phys. Rev. D* **104**, 073008 (2021).
- [42] M. B. Barbaro, *PoS NuFact2021*, 007 (2022).
- [43] J. M. Franco-Patino, M. B. Barbaro, J. A. Caballero, and G. Megias, *PoS NuFact2021*, 227 (2022).
- [44] J. M. Franco-Patino, S. Dolan, R. Gonzalez-Jimenez, M. B. Barbaro, J. A. Caballero, and G. D. Megias, [arXiv:2304.01916](https://arxiv.org/abs/2304.01916).
- [45] A. De Pace, M. Nardi, W. M. Alberico, T. W. Donnelly, and A. Molinari, *Nucl. Phys. A* **726**, 303 (2003).
- [46] I. Ruiz Simo, J. E. Amaro, M. B. Barbaro, A. De Pace, J. A. Caballero, and T. W. Donnelly, *J. Phys. G: Nucl. Part. Phys.* **44**, 065105 (2017).
- [47] R. Rosenfelder, *Ann. Phys. (NY)* **128**, 188 (1980).
- [48] B. D. Serot and J. D. Walecka, in *Advances in Nuclear Physics*, edited by J. W. Negele and E. Vogt (Plenum, New York, 1986), Vol. 16.
- [49] K. Wehrberger, *Phys. Rep.* **225**, 273 (1993).
- [50] G. D. Megias, J. E. Amaro, M. B. Barbaro, J. A. Caballero, and T. W. Donnelly, *Phys. Rev. D* **94**, 013012 (2016).
- [51] G. D. Megias, J. E. Amaro, M. B. Barbaro, J. A. Caballero, T. W. Donnelly and I. R. Simo, *Phys. Rev. D* **94**, 093004 (2016).
- [52] G. D. Megias, M. B. Barbaro, J. A. Caballero, J. E. Amaro, T. W. Donnelly, I. Ruiz Simo and J. W. Van Orden, *J. Phys. G* **46**, 015104 (2019).
- [53] M. V. Ivanov, A. N. Antonov, G. D. Megias, J. A. Caballero, M. B. Barbaro, J. E. Amaro, I. Ruiz Simo, T. W. Donnelly and J. M. Udias, *Phys. Rev. C* **99**, 014610 (2019).
- [54] V. L. Martinez-Consentino, I. R. Simo, and J. E. Amaro, *Phys. Rev. C* **104**, 025501 (2021).
- [55] V. L. Martinez-Consentino, J. E. Amaro and I. Ruiz Simo, *Phys. Rev. D* **104**, 113006 (2021).
- [56] V. L. Martinez-Consentino and J. E. Amaro, *Phys. Rev. D* **108**, 113006 (2023).
- [57] P. R. Casale, J. E. Amaro, and M. B. Barbaro, *Symmetry* **15**, 1709 (2023).
- [58] E. Hernandez, J. Nieves, and M. Valverde, *Phys. Rev. D* **76**, 033005 (2007).
- [59] I. R. Simo, C. Albertus, J. E. Amaro, M. B. Barbaro, J. A. Caballero, and T. W. Donnelly, *Phys. Rev. D* **90**, 053010 (2014).
- [60] V. L. Martinez-Consentino, J. E. Amaro, P. R. Casale and I. Ruiz Simo, *Phys. Rev. D* **108**, 013007 (2023).
- [61] I. Ruiz Simo, J. E. Amaro, M. B. Barbaro, A. De Pace, J. A. Caballero, G. D. Megias, and T. W. Donnelly, *Phys. Lett. B* **762**, 124 (2016).